The Abdus Salam International Centre for Theoretical Physics

United Nations Educational, Scientific and Cultural Organization

IAEA
International Atomic Energy Agency

1932-3

Winter College on Micro and Nano Photonics for Life Sciences

11 - 22 February 2008

Optics at the nanoscale: an overview (part I, II and III)

Oscar Martinez

Universidad de Buenos Aires
Buenos Aires
Argentina

Introduction to Nano-Optics

- Oscar Eduardo Martínez
- Laboratorio de Electrónica Cuántica
- Departamento de Física
- Facultad de Ciencias Exactas y Naturales
- Universidad de Buenos Aires
- www.lec.df.uba.ar

Desaparecidos Missing 1976-1983

Maria de los Milagros BALERIANI
Gustavo Delfor GARCIA CAMPANNINI
Maria Estela GENTILE
Matilde ITZIGZHON
Ana Patricia STEINBERG
Antonio MISETICH
Eduardo Alfredo PASQUINI
Jorge Luis BADILLO
Jorge BONAFINI
Federico Eduardo ALVAREZ ROJAS
Gabriela CARABELLI
Enrique Erenesto ESPECHE
Alfredo Antonio GIORGI
Jorge Israel GORFINKEL
Guillermo Claudio VARGAS AIGNASE
Graciela Mabel BARROCA
Daniel Eduardo BENDERSKY
Susana Flora GRYNBERG
Julia Natividad HUARQUE
Ignacio IKONICOFF
Federico Gerardo LUDDEN
Eduardo Alberto MARTINEZ
Daniel Lazaro RUS
Gerardo STREJILEVICH

Outline

1. Introduction and motivations
2. Localization vs. resolution
3. Nonlinear approach
4. Near field approach
5. Newcomers
   – Short wavelength sources
   – Superlenses

Outline

1. Introduction and motivations
2. Localization vs. resolution
3. Nonlinear approach
4. Near field approach
5. Newcomers
   – Short wavelength sources
   – Superlenses

Advances in optical microscopy

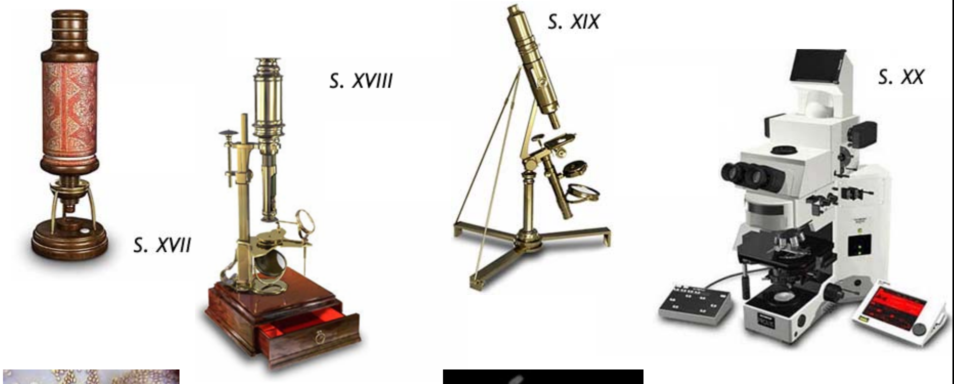

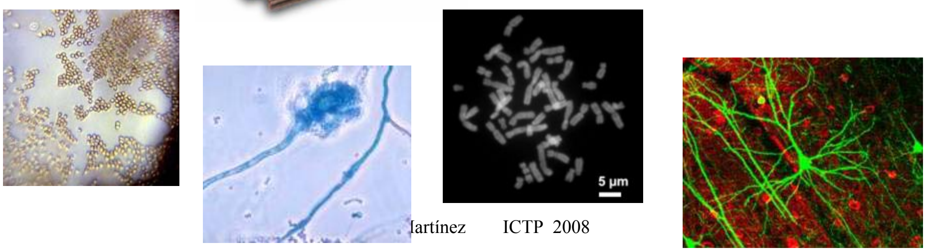

Confocal Principle

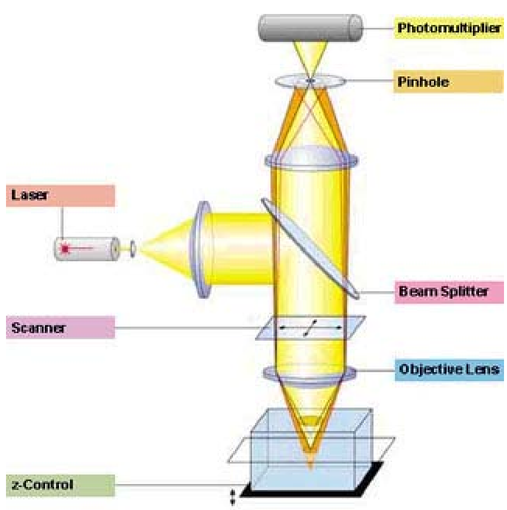

Other options

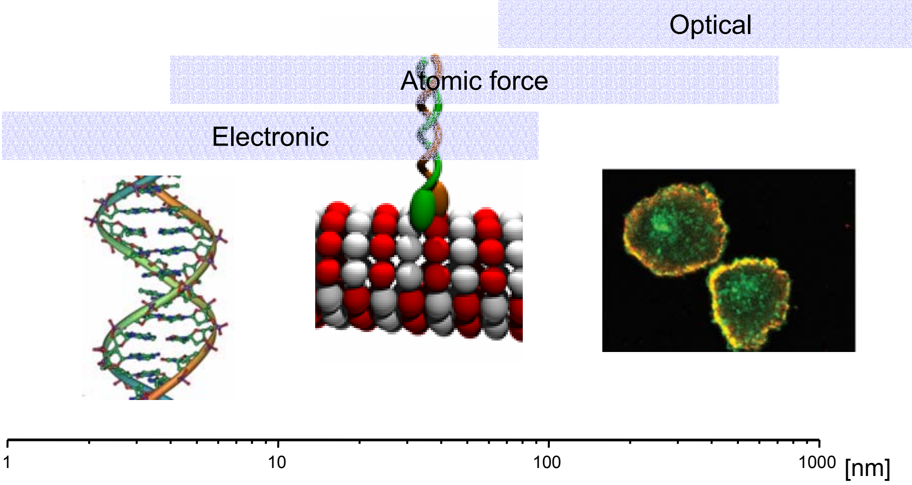

SPATIAL RESOLUTION VS.CHEMICAL INFORMATION

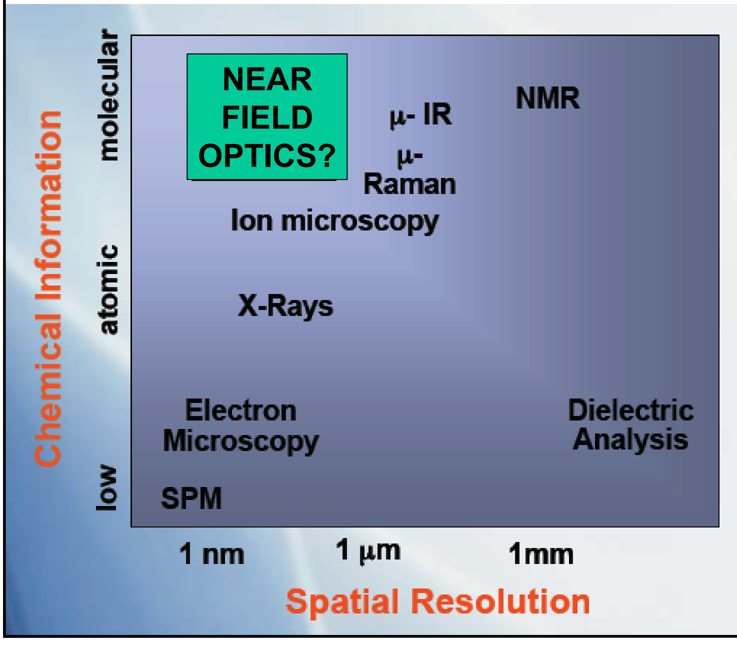

S. Stranick, NIST

1880's: Rigorous Discussion of Resolution in Optical Microscopy

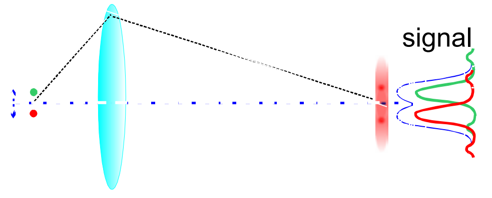

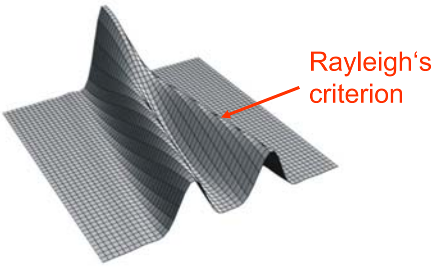

1880's: Rigorous Discussion of Resolution in Optical Microscopy

- Conclusion:
  – you cannot resolve two points closer than about ½ wavelength
  –When imaging in the far field

$$\mathbf{E}(\mathbf{r},t) = \sum_{\sigma,k_x,k_y} \mathbf{E}_\sigma(k_x,k_y)\exp\left(ik_z z + ik_x x + ik_y y - i\omega t\right)$$

where we choose the axis of the lens to be the *z*-axis. Maxwell's equations tell us that,

$$k_z = +\sqrt{\omega^2 c^{-2} - k_x^2 - k_y^2}, \quad \omega^2 c^{-2} > k_x^2 + k_y^2,$$

$$k_z = +i\sqrt{k_x^2 + k_y^2 - \omega^2 c^{-2}}, \quad \omega^2 c^{-2} < k_x^2 + k_y^2.$$

Since the propagating waves are limited

$$k_x^2 + k_y^2 < \omega^2 c^{-2}$$

the maximum resolution in the image can never be greater than,

$$\Delta \approx \frac{2\pi}{k_{\max}} = \frac{2\pi c}{\omega} = \lambda$$

Point spread function PSF

A "point" source yields a blurred image

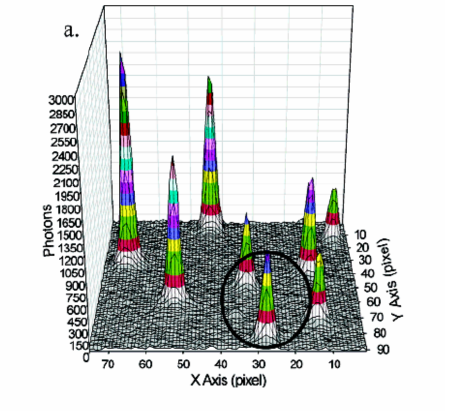

image of several individual Cy3-dyes immobilized onto glass coverslip.

Fluorescence Imaging with One Nanometer Accuracy: Application to Molecular Motors. Acc. Chem. Res. **2005,** 38, 574-582. AHMET YILDIZ AND PAUL R. SELVIN

Outline

1. Introduction and motivations
2. Localization vs. resolution
3. Nonlinear approach
4. Near field approach
5. Newcomers
   – Short wavelength sources
   – Superlenses

Localization vs. resolution

- Localization techniques
- Tracking
- 3D imaging

Localization

Taking a picture of a point source

Changing the pixel size

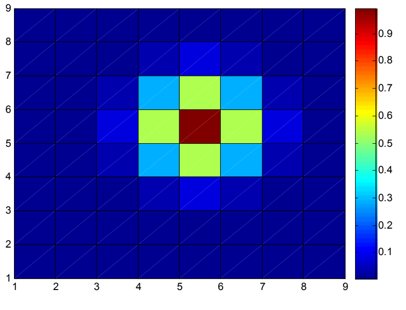

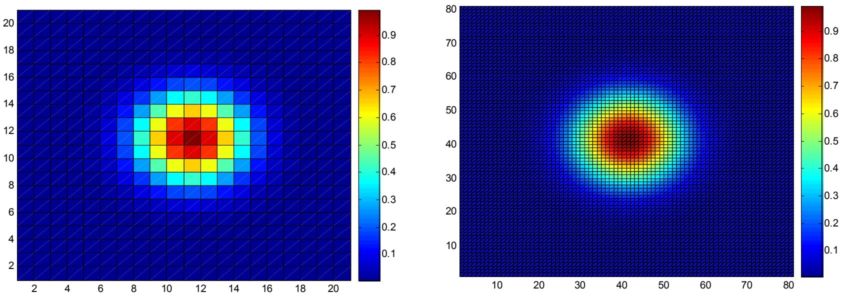

Increasing the noise

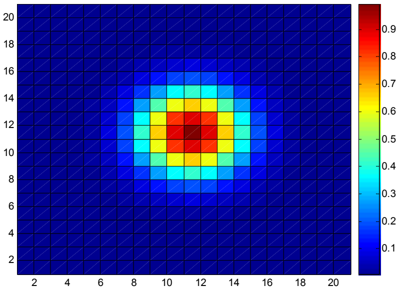

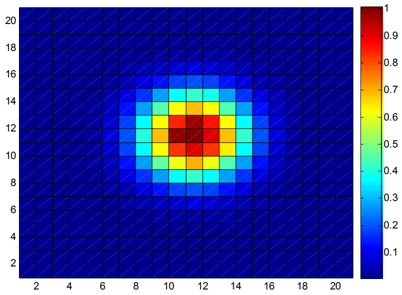

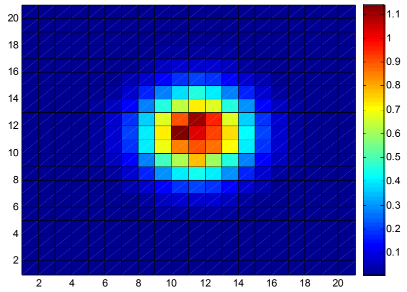

Limits

$$\sigma_{\mu_i} = \sqrt{\left(\frac{s_i^2}{N} + \frac{a^2/12}{N} + \frac{8\pi\, s_i^4 b^2}{a^2 N^2} \right)}$$

s : standard deviation of the Gaussian distribution = 1/2.2 of the PSF width, *a* is the pixel size, *b* is background and *N* is number of collected photons.

first term: photon noise,

second term: effect of finite pixel size of the detector,

last term: effect of background.

Thompson, R. E.; Larson, D. R.;Webb, W. W. Precise nanometer localization analysis for individual fluorescent probes. Biophys. J.**2002**, 82(5), 2775-2783.

Localization

Pixelated image of several individual Cy3-dyes immobilized onto glass coverslip. Dyes were imaged by using objectivetype TIR with 0.5-s integration time.

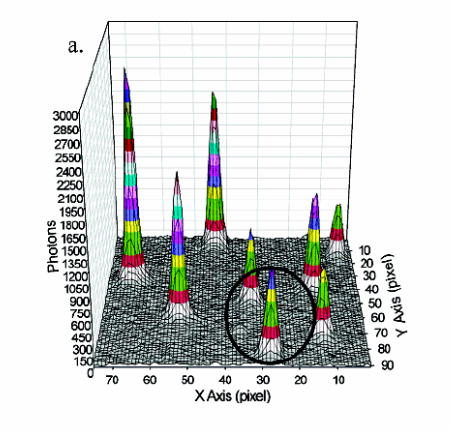

Fluorescence Imaging with One Nanometer Accuracy: Application to Molecular Motors. Acc. Chem. Res. **2005,** 38, 574-582. AHMET YILDIZ AND PAUL R. SELVIN

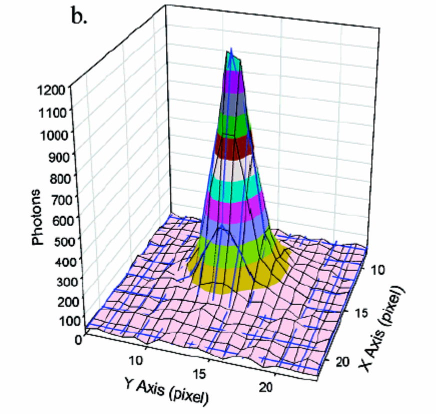

(B) The PSF circled in (A) has a width of 287 nm, and the SNR of 32. A Gaussian curve-fit (solid blue line)yielded 1.3 nm precision in the center localization.

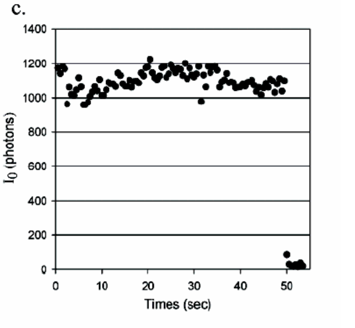

(C) The dye lasted for 50 s and photobleached in a single step that indicates the image contains a single dye.

Acc. Chem. Res. **2005,** 38, 574-582. AHMET YILDIZ AND PAUL R. SELVIN

Calibration

Acc. Chem. Res. **2005,** 38, 574-582.
AHMET YILDIZ AND PAUL R. SELVIN

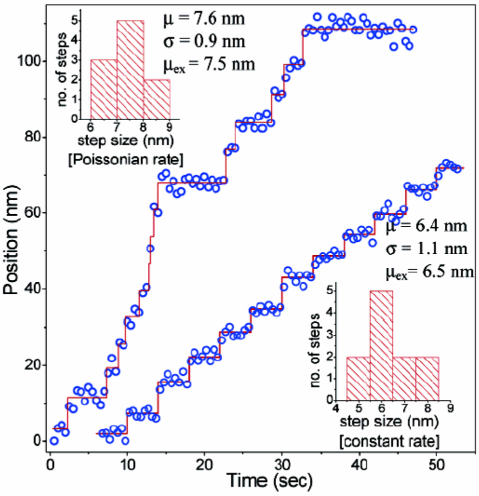

(D) The PSF center versus time graph. The sample was moved with a nanometric stage with 6.5 nm increments either at a constant rate or a Poisson-distributed rate. Red lines show the average position between each step. Steps are visually separable and are determined with 1 nm precision (Ǘ), and the accuracy [difference between the measured step size via PSF fitting (Ì) and the expected step size (Ìex) based on the calibrated stage] is better than 1 nm.

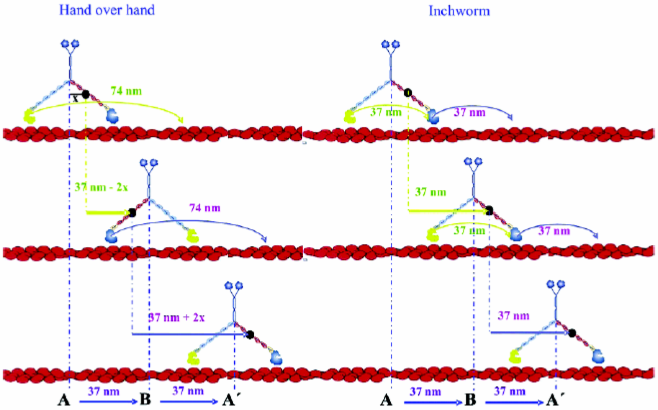

Hand-over-hand model vs Inchworm odel for myosin V. In the hand-over-hand model, the rear head passes by the front head, translating a total of 74 nm, while the front head stays stationary. Therefore, heads move alternating 74 and 0 nm steps. If the dye is on the light chain, it moves 37 - 2 x, followed by 37 + 2 xnm, where xis the distance between the dye and the center. In the inchworm model, the dye moves 37 nm regardless to where it is labeled.

Acc. Chem. Res. **2005,** 38, 574-582. AHMET YILDIZ AND PAUL R. SELVIN

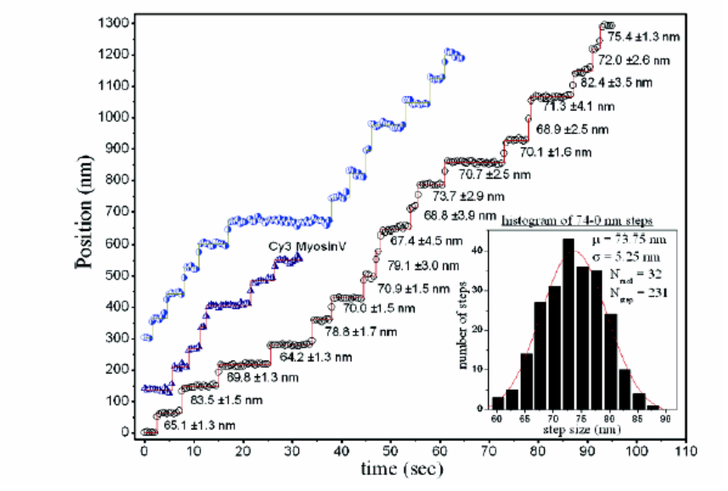

Stepping traces of three different myosin V molecules displaying 74 nm steps, and histogram of a total of 32 myosin V's taking 231 steps. Traces are for BR-labeled myosin V unless noted as Cy3.

Acc. Chem. Res. **2005,** 38, 574-582. AHMET YILDIZ AND PAUL R. SELVIN

photoactivated localization microscopy (PALM)

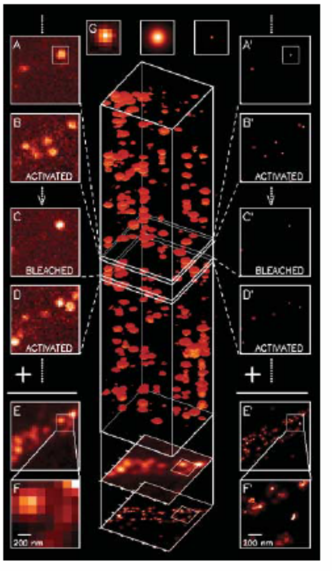

The principle behind PALM. A sparse subset of PA-FP molecules that are attached to proteins of interest and then fixed within a cell are activated (A and B) with a brief laser pulse at λ_{act} = 405 nm and then imaged at λ_{exc} = 561 nm until most are bleached (C). This process is repeated many times (C and D) until the population of inactivated, unbleached molecules is depleted. Summing the molecular images across all frames results in a diffraction-limited image (E and F). However, if the location of each molecule is first determined by fitting the expected molecular image given by the PSF of the microscope [(G), center] to the actual molecular image [(G), left], the molecule can be plotted [(G), right] as a Gaussian that has a standard deviation equal to the uncertainty $\sigma_{x,y}$ in the fitted position. Repeating with all molecules across all frames (A¶ through D¶) and summing the results yields a superresolution image (E¶ and F¶) in which resolution is dictated by the uncertainties sx,y as well as by the density of localized molecules. Scale: 1x1 µm in (F) and (F¶), 4x4 µm elsewhere.

Eric Betzig *et al.*, **313** *Science* , 1642 (2006);

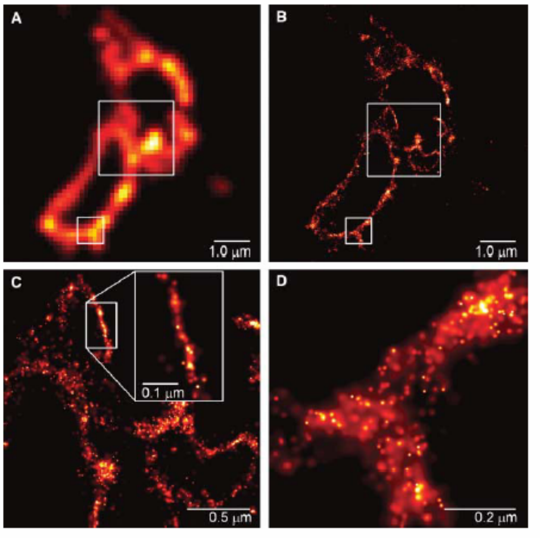

Comparative summed-molecule TIRF (A) and PALM (B) images of the same region within a cryoprepared thin section from a COS-7 cell expressing the lysosomal transmembrane protein CD63 tagged with the PA-FP Kaede. The larger boxed region in (B), when viewed at higher magnification (C) reveals smaller associated membranes that may represent interacting lysosomes or late endosomes that are not resolvable by TIRF. In a region where the section is nearly orthogonal to the lysosomal membrane, the most highly localized molecules fall on a line of width ~10 nm (inset). In an obliquely cut region [(D), from the smaller boxed region in (B)], the distribution of CD63 within the membrane plane can be discerned.

Eric Betzig *et al.*, **313** *Science* , 1642 (2006);

Outline

1. Introduction and motivations
2. Localization vs. resolution
3. Nonlinear approach
4. Near field approach
5. Newcomers
   - Short wavelength sources
   - Superlenses

WAVE EQUATION

$$\nabla^2 \vec{E} - \frac{1}{c^2}\frac{\partial^2 \vec{E}}{\partial t^2} = \frac{4\pi}{c^2}\frac{\partial^2 \vec{P}}{\partial t^2}$$

P is a source

NONLINEAR OPTICS: NAIVE APROACH

LOSSLESS, DISPERSIONLESS

$$P(t) = \chi^{(1)} E(t) + \chi^{(2)} E^2(t) + \chi^{(3)} E^3(t) + \ldots$$

$$P(t) = P^{(1)}(t) + P^{(2)}(t) + P^{(3)}(t) + \ldots$$

See lecture Prof. Bertolotti

Example: 2nd order term. Monochromatic wave.

$$P^{(2)}(t) = \chi^{(2)} (E e^{i\omega t} + cc)^2$$

$$P^{(2)}(t) = \chi^{(2)} 2EE^* + \chi^{(2)} [E^2 e^{i2\omega t} + cc]$$

d.c. field

Source at 2ω

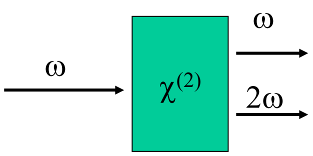

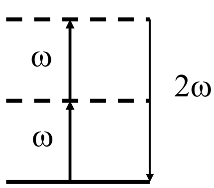

PROCESS	ORDER	$-\omega_\sigma;\omega_1,\omega_2,\ldots\omega_n$
d.c.Kerr effect	3	$-\omega;0,0,\omega$
d.c.induced 2^{nd} harmonic generation	3	$-2\omega;0,\omega,\omega$
3^{rd} harmonic generation	3	$-3\omega;\omega,\omega,\omega$
4 wave mixing	3	$-\omega_4;\omega_1,\omega_2,\omega_3$
3^{rd} order sum frequency mixing	3	$-\omega_3;\omega_1,\omega_2,\omega_2$
3^{rd} order difference frequency mixing	3	$-\omega_3;-\omega_1,\omega_2,\omega_2$
Coherent anti-Stokes Raman scattering	3	$-\omega_{AS};\omega_P,\omega_P,-\omega_S$
stimulated Raman and Brillouin scattering	3	$-\omega_S;\omega_P,-\omega_P,\omega_S$
Optical Kerr effect, intensity dependent refractive index	3	$-\omega;\omega,-\omega,\omega$
2 photon absorption	3	$-\omega;-\omega,\omega,\omega$
N photon absorption	2N-1	$-\omega;-\omega,\ldots-\omega,\omega,\ldots\omega$
Nth harmonic generation	N	$-N\omega;\omega,\ldots\omega$

See lecture Prof. Rigneault

Simultaneous Imaging on Multi-Photon Excitation Fluorescence and Third Harmonic using a Diode-Pumped Nd:Glass Laser

Juerg Aus der Au, Virgis Barzda, David N. Fittinghoff, Xylar S. Asay-Davis, Tim J. Foley, and Jeffrey A. Squier
Department of Chemistry and Biochemistry, University of California, San Diego, La Jolla, CA 92093-0339, USA

Experimental Setup

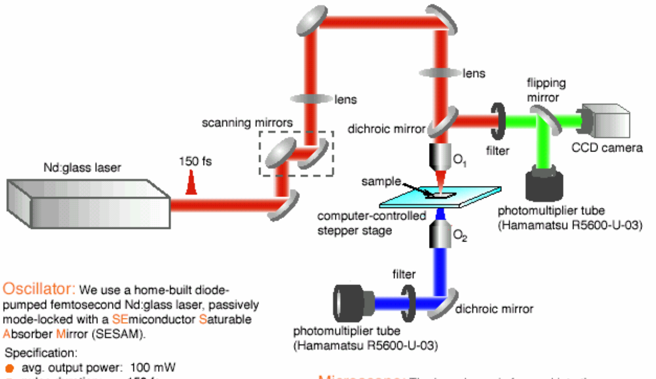

Oscillator: We use a home-built diode-pumped femtosecond Nd:glass laser, passively mode-locked with a SEmiconductor Saturable Absorber Mirror (SESAM).

Specification:
- avg. output power: 100 mW
- pulse duration: 150 fs
- repetition rate: 95 MHz
- laser wavelength: 1064 nm
- pump power: 1.5 W
- gain material: Nd:silicate glass (Schott LG6870)

The emitting wavelength of the Nd:glass laser is optimally matched to the water absorption windows both at the fundamental and third harmonic wavelength, as well as to the onset of UV absorption within the specimen and collection optics.

Microscope: The laser beam is focused into the sample by a microscope objective O_1 (Zeiss A-Plan, 40x, NA 0.65). The specimen is mounted on a computer-controlled stepper stage, which controls the axial position to 0.1 m. The focal point is scanned in the X-Y plane by two galvanometric scanners. The generated THG radiation at 355 nm is collected in forward direction by a second objective O_2 (Fluar, 20x, NA 0.70), filtered, and measured by a photomultiplier tube (PMT).

The two-photon excitation fluorescence signal is detected in backward direction by either a second PMT or a CCD.

THG Images of biological specimens

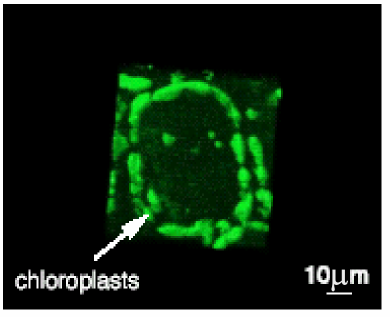

Three-dimensional reconstruction of a leaf section (*Clivia mineata*). The picture shows the view through the top of the leaf surface, revealing the chloroplasts.

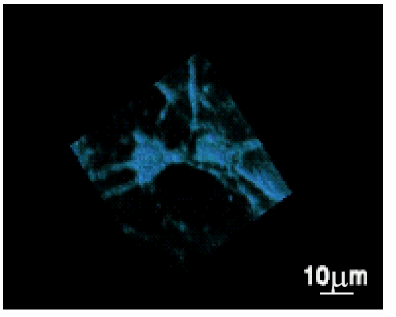

Three-dimensional reconstruction of a single neuron cell.

Stomata & chloroplasts

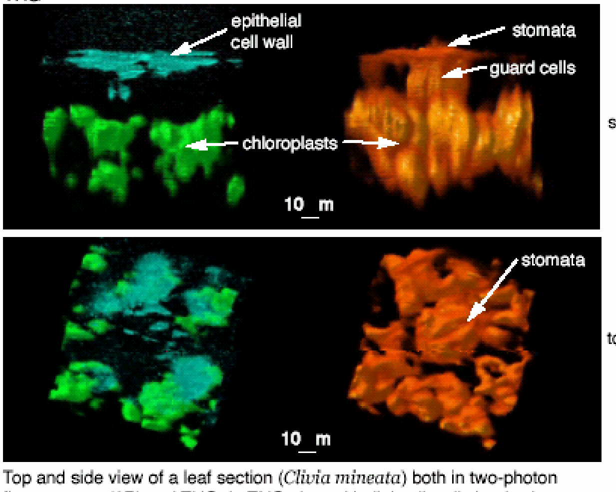

Top and side view of a leaf section (*Clivia mineata*) both in two-photon fluorescence (2P) and THG. In THG, the epithelial cell wall clearly shows up (gray coloration). On the other hand, the guard cells around the stomata appear in the 2P image, but not in THG (laser beam parallel to interface).

STED microscopy reveals that synaptotagmin remains clustered after synaptic vesicle exocytosis

Katrin I. Willig1*, Silvio O. Rizzoli2*, Volker Westphal1, Reinhard Jahn2 & Stefan W. Hell1

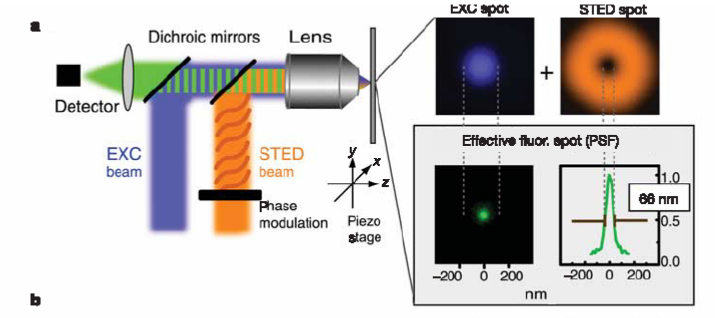

Vol 440|13 April 2006|doi:10.1038/nature04592

See lecture Prof. Westphal

Nonliear nanopatterning

The nonlinearity can be anywhere

THE SETUP

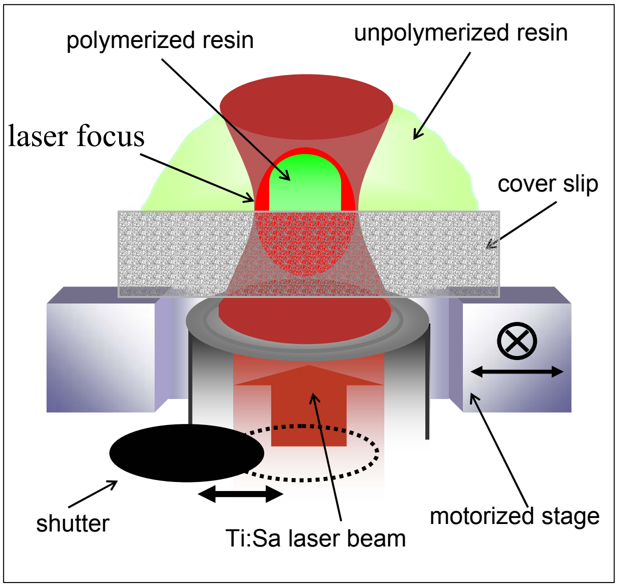

ART FAIR

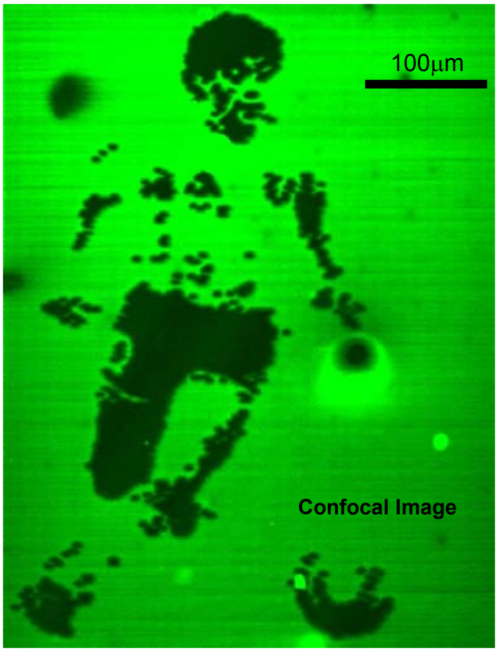

We can make fluorescent lithography on standard coverslips

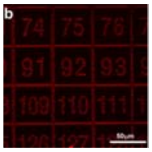

The fluorescent structure are compatible with cell cultures

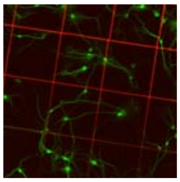

The can replace Si substrates reducing the price and production time by orders of magnitude

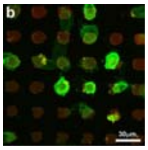

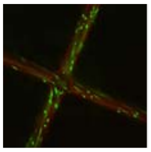

How small can the pattern be?

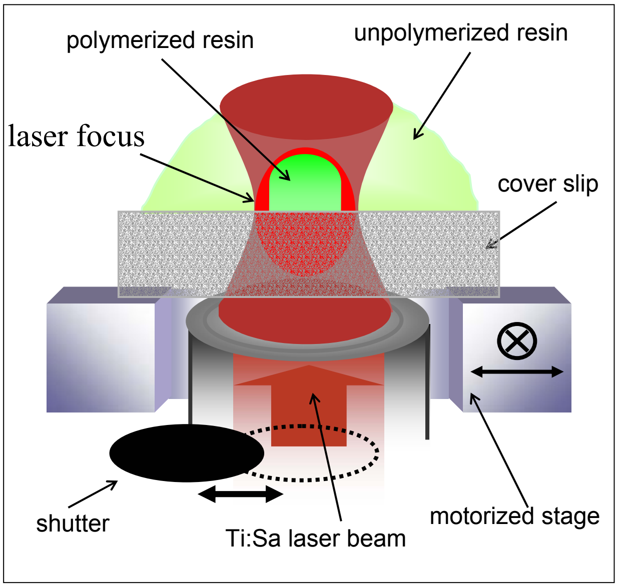

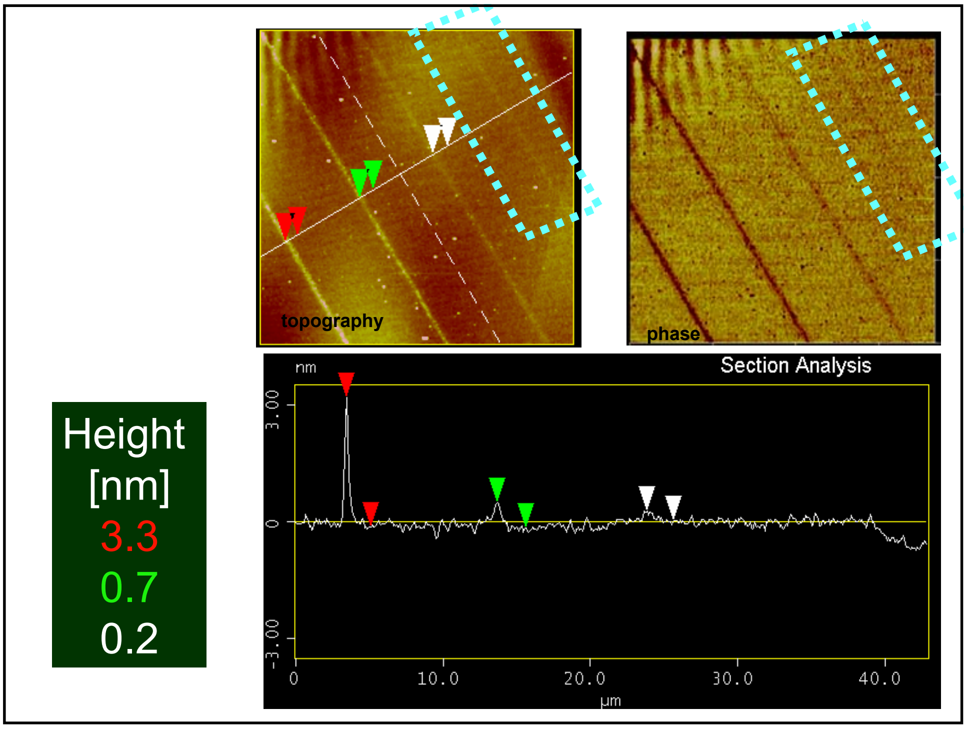

The polymer growth starts on the surface of the substrate

AFM Phase image

AFM Topographic image

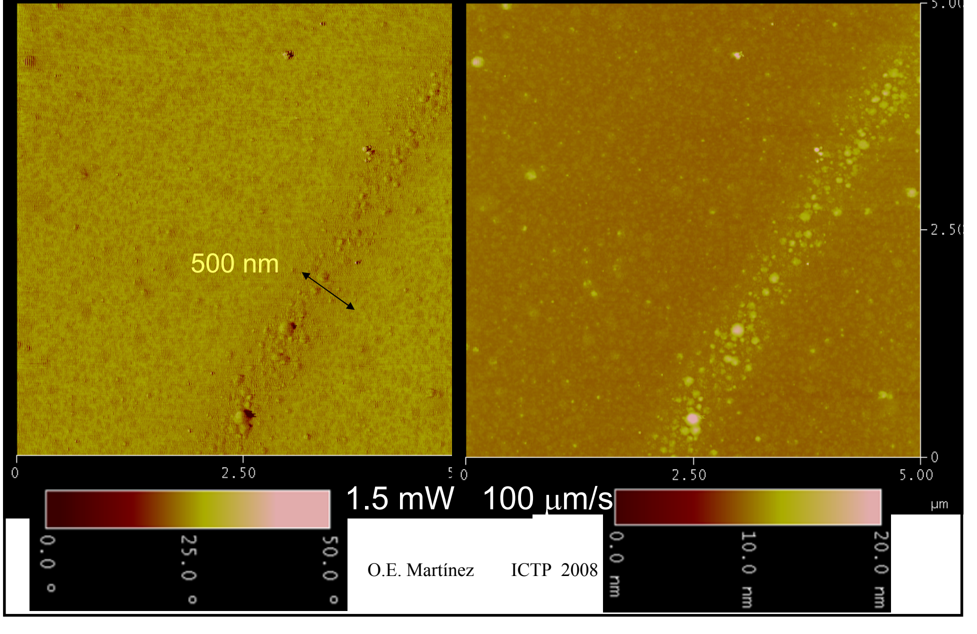

O.E. Martínez ICTP 2008

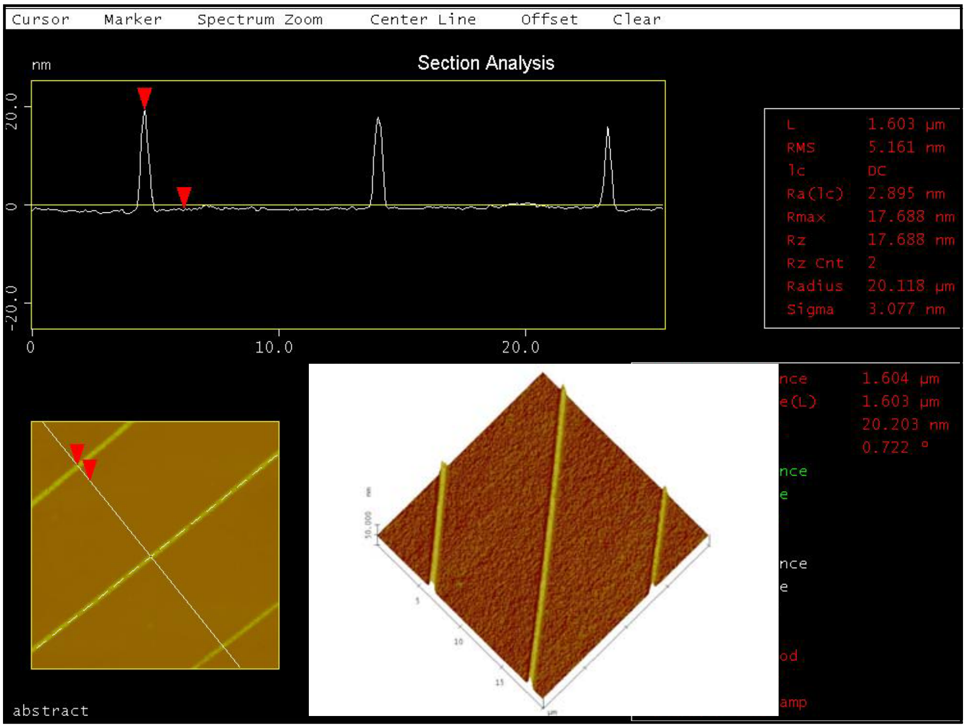

Confocal image

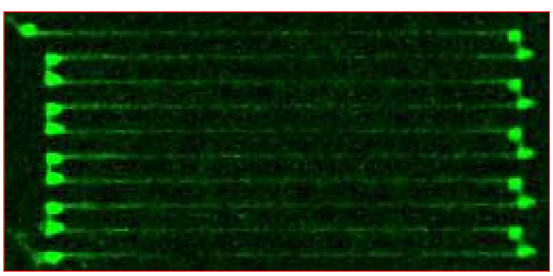

height < 20 nm
length = 100 µm
separation = 5 µm

Nonlinearity= percolation

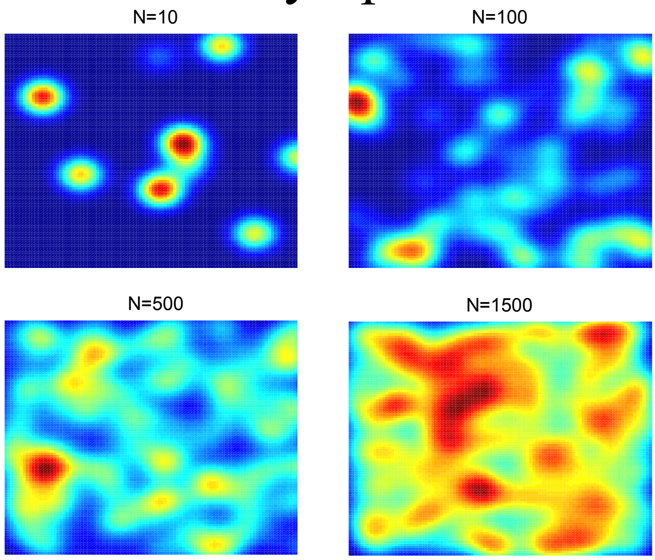

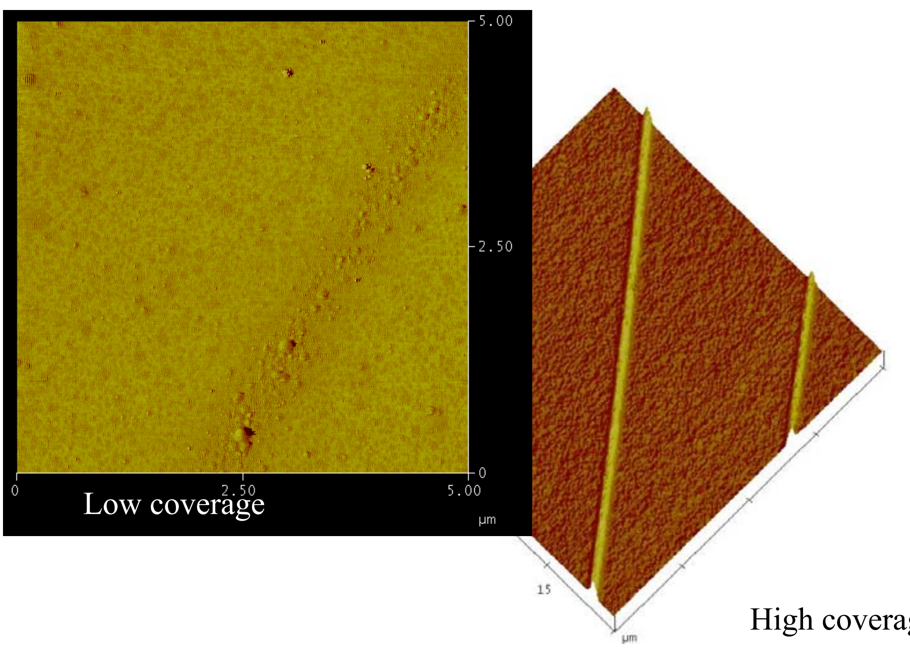

High coverage

Outline

1. Introduction and motivations
2. Localization vs. resolution
3. Nonlinear approach
4. Near field approach
5. Newcomers
   - Short wavelength sources
   - Superlenses

Near field approach

- **Are there limitations?**
- **The plasmonic highway**
- **Imaging**
- **New enhancement geometries**
- **Is imaging the only motivation?**

Near Field

$$\mathbf{E}(\mathbf{r},t)=\sum_{\sigma,k_x,k_y}\mathbf{E}_\sigma\left(k_x,k_y\right)\exp\left(ik_z z+ik_x x+ik_y y-i\omega t\right)$$

Now we want to see the components

$$k_z=+i\sqrt{k_x^2+k_y^2-\omega^2c^{-2}},\qquad \omega^2c^{-2}<k_x^2+k_y^2.$$

Measure:Im(ε)

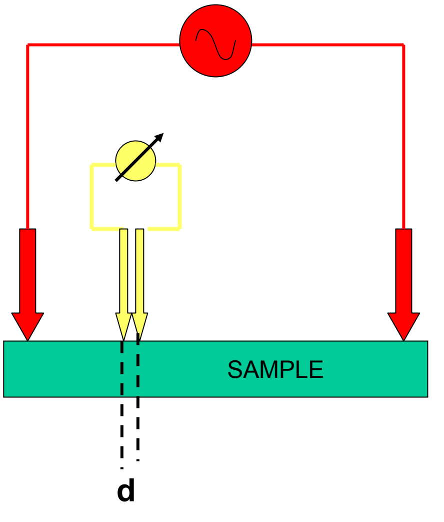

For

F=1kHz

d=3mm

Yields

λ/d=100,000,000

The Basic Ideas

Goal: Measuring the nonpropagating fields that contain high spatial frequencies at the surface of the sample

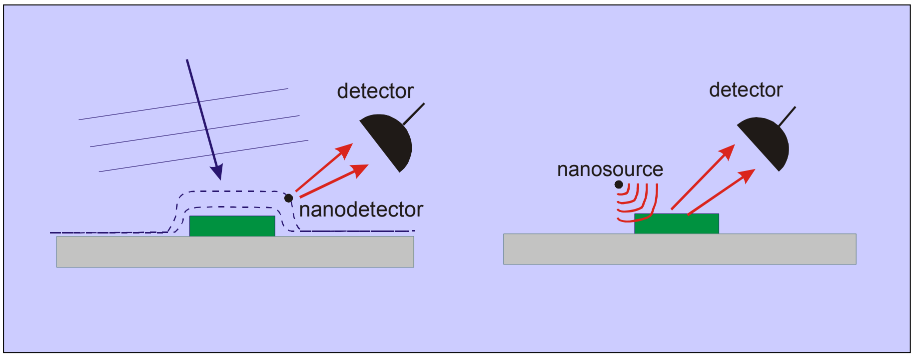

See lecture Prof. Subramaniam

Vahid Sandoghdar

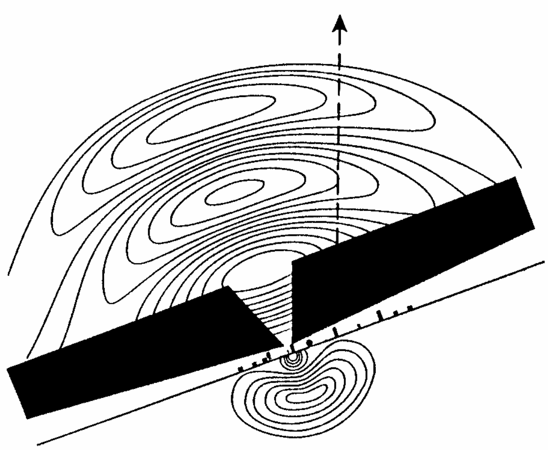

Fig. 1. The concept of SNOM.

D. W. Pohl, 1991

TIPS

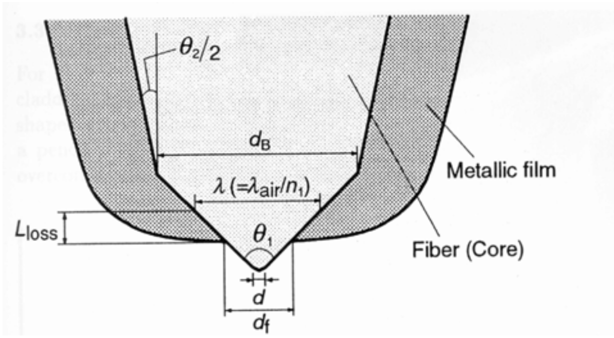

Limited in size by the skin depth

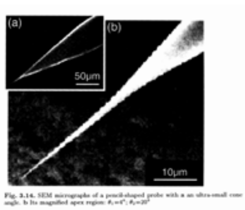

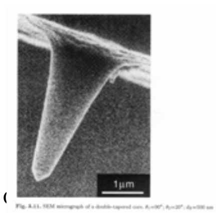

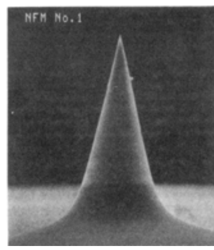

Near field approach

- **Are there limitations?**
- **The plasmonic highway**
- **Imaging**
- **New enhancement geometries**
- **Is imaging the only motivation?**

Optical properties of metal nanoparticles

Polarizability of a sphere

$$\alpha(\omega) \propto \frac{\varepsilon(\omega)-\varepsilon_m}{\varepsilon(\omega)+2\varepsilon_m}$$

for $\varepsilon(\omega) = -2\varepsilon_m$

→ Resonance

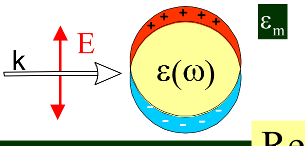

Enhancement factor:= $\dfrac{\mathrm{Re}(\varepsilon)}{\mathrm{Im}(\varepsilon)}$

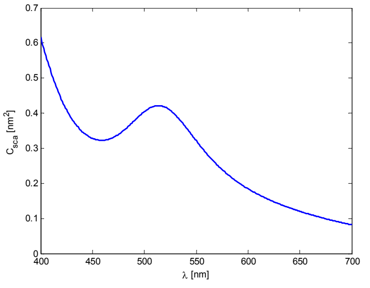

full electrodynamic calculation: Mie theory

G. Mie, *Ann. Phys.* **25** (1908)

Scattering and Plasmon Resonances of Metal Particles

Dark-field image of silver nanoparticles

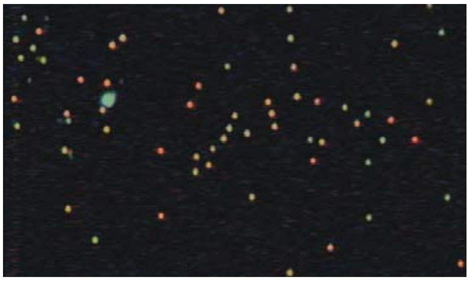

Plasmon resonance of a single nanoparticle

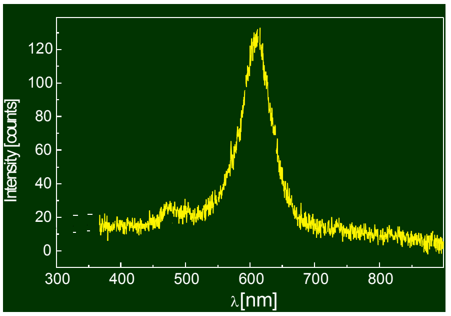

Vahid Sandoghdar

solution: direct optical detection and spectroscopy

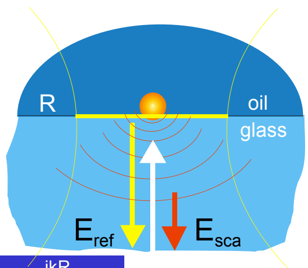

$$E_{ref} \sim re^{-i\pi/2}E_{inc}$$

$$E_{sca} = sE_{inc} \sim D^3 \frac{\varepsilon - \varepsilon_m}{\varepsilon + 2\varepsilon_m}\frac{e^{ikR}}{R}E_{inc}$$

r: Fresnel field reflectivity

$\pi/2$: Gouy phase/2

$$I_{det} = \left|E_{ref} + E_{sca}\right|^2 = \left|E_{inc}\right|^2 \left\{r^2 + |s|^2 - 2r|s|\sin\varphi\right\}$$

scales as D^3

φ: scattering phase: $s = |s|e^{i\varphi}$

Plasmon Spectra of Single Gold Nanoparticles

$$\sigma(\lambda) = \frac{I_m(\lambda) - I_r(\lambda)}{I_r(\lambda)}$$

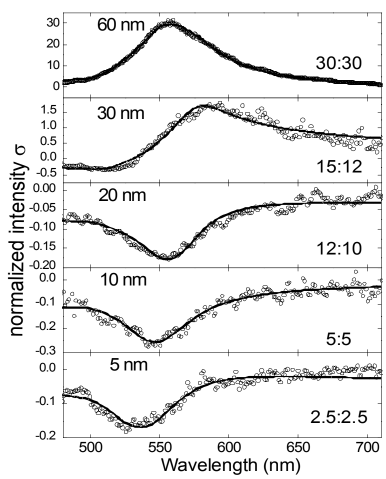

K. Lindfors, T. Kalkbrenner, P. Stoller, & V. Sandoghdar, *PRL* **93**, 037401-1 (2004).

dephasing mechanisms

- Emission of electrons occurs on a time scale of 4-6 fs and is only observed for small nanoparticles (< 1nm) which are interacting with strong light fields.
- Landau-damping describes the generation of electronhole-pairs . For low SPP energies intraband- and for higher energies interbandtransition are observed. For small nanoparticles a 1/R-dependence of the inverse dephasing time is predicted .

dephasing mechanisms

- Surface scattering: when the free mean path of the electrons is of the same order of magnitude as the nanoparticle diameter. Also, a 1/Rdependence.
- Chemical interface damping (CID): the tunneling of the oscillating electrons into and out of adsorbate or surface states. Because of the surface-sensitivity, a 1/R-dependence is predicted.

dephasing mechanisms

- Radiation damping: an efect which is due to the emission of photons. It is proportional to the volume of the nanoparticles and dominates in large particles with R > 20 nm.
- Electron-electron-scattering: the dissipation of the SPP energy among the electrons which takes place after about 500 fs
- Electron-phonon-scattering. On a timescale of about 1 ps the energy is transferred from the hot electrons to the lattice of the ion cores].

Measurement of the size dependent dephasing time of surface plasmon excitation in gold nanoparticles C. Hendrich, F. Hubenthal, and F. Tr¨ager. Private commun

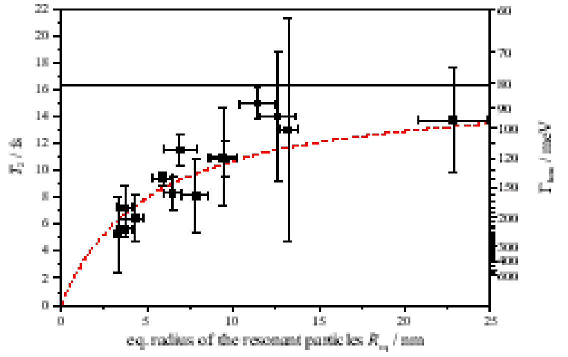

FIG. 3: Dephasing time (left axis) and homogeneous line width (right axis) as a function of the equivalent radius of the gold nanoparticles. The solid line represents the dephasing time of $T_2 = 16.3$ fs calculated from ϵ_{bulk} and the dashed line a fit of the $1/R_{eq}$-dependence from eq. (2) which is predicted by several models.

Near field approach

- **Are there limitations?**
- **The plasmonic highway**
- **Imaging**
- **New enhancement geometries**
- **Is imaging the only motivation?**

FIELD ENHANCED IMAGING

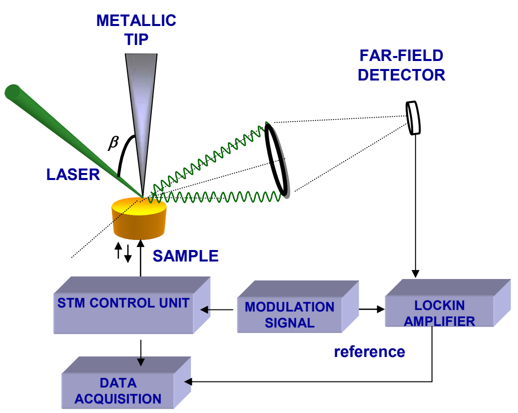

Scattered light vs. distance

Approach curves

Scattered light while scanning

Ultrahigh resolution optical images

A.V.Bragas and O. E. Martínez, Optics Letters 25 (2000) pp.

GRAPHITE (HOPG)

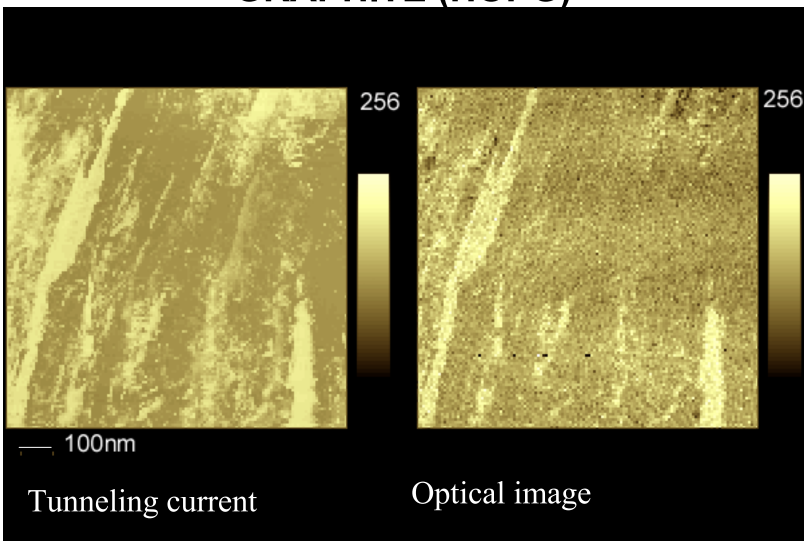

Constant hight scan. Optical Step response: 3nm

Backscattering geometry

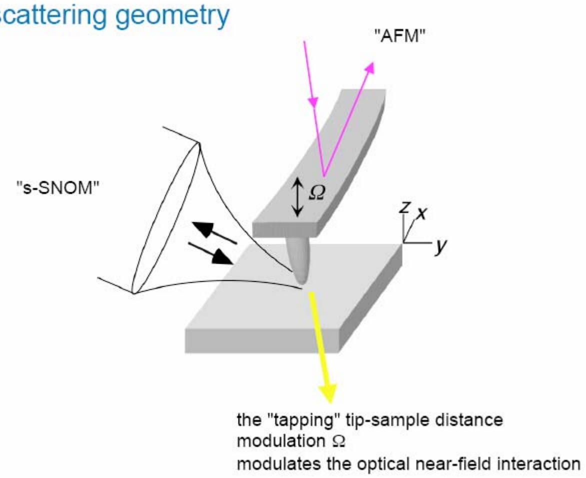

s-SNOM with heterodyne detection of backscattering

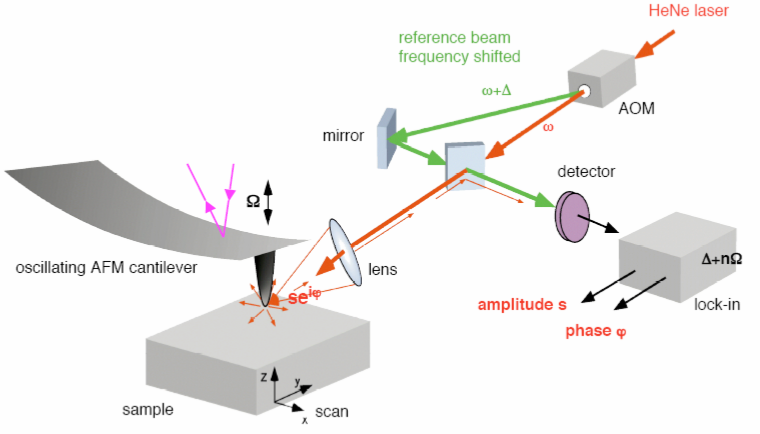

R. Hillenbrand, F. Keilmann, Phys. Rev. Lett. **80**, 3029 (2000)

Material-dependent, λ-independent near-field contrast

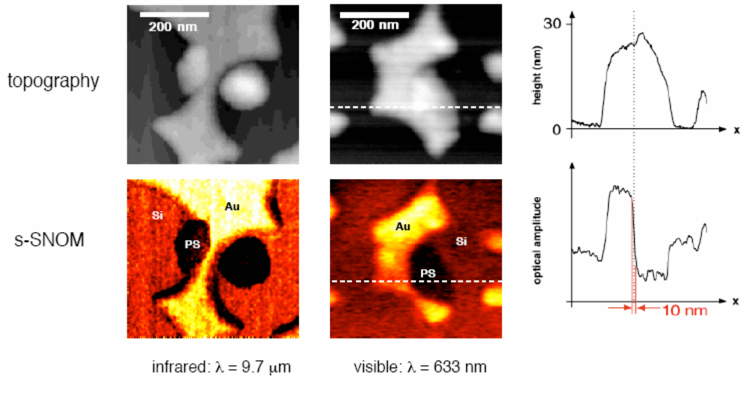

T. Taubner, R. Hillenbrand, F. Keilmann, J. Microscopy **210**, 311 (2003)

Particle with quadrupolar mode

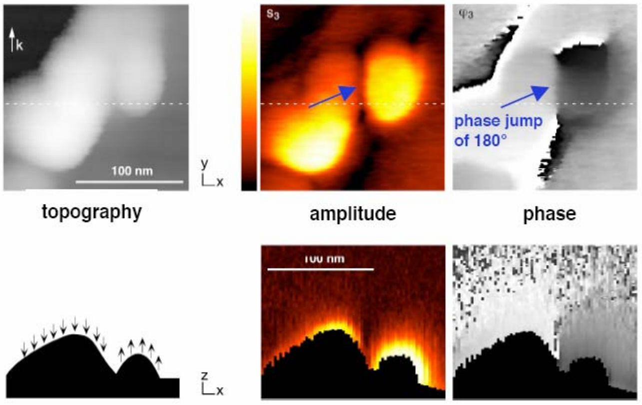

R. Hillenbrand, F. Keilmann, Appl. Phys. B **79** (2001)

Enhancement: sources

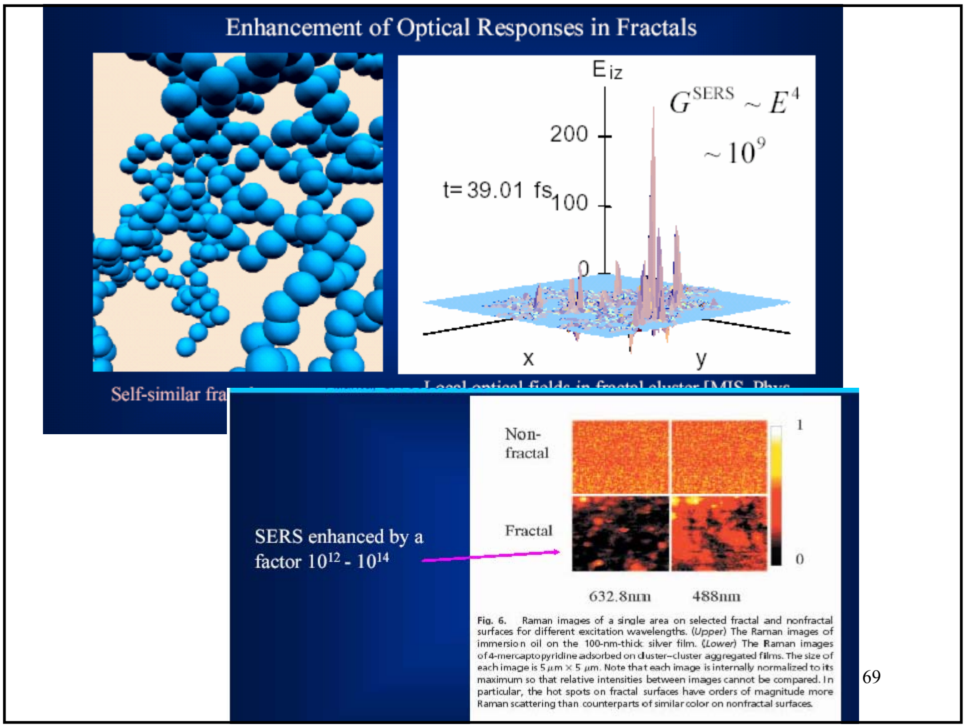

Enhancement of Optical Responses in Fractals
E iz
$G^{SERS} \sim E^4$
$\sim 10^9$
200
t= 39.01 fs
100
0
x
y
Self-similar fra
SERS enhanced by a factor 10^{12} - 10^{14}
Non-fractal
Fractal
1
0
632.8nm
488nm
Fig. 6. Raman images of a single area on selected fractal and nonfractal surfaces for different excitation wavelengths. (Upper) The Raman images of immersion oil on the 100-nm-thick silver film. (Lower) The Raman images of 4-mercaptopyridine adsorbed on cluster–cluster aggregated films. The size of each image is 5 μm × 5 μm. Note that each image is internally normalized to its maximum so that relative intensities between images cannot be compared. In particular, the hot spots on fractal surfaces have orders of magnitude more Raman scattering than counterparts of similar color on nonfractal surfaces.
69

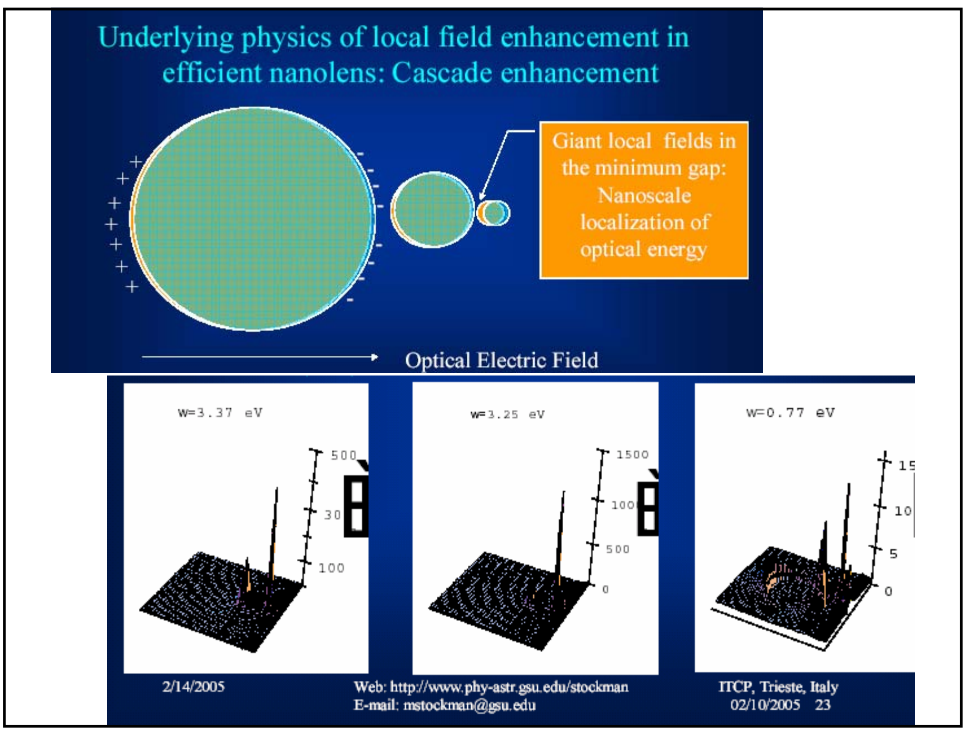

Underlying physics of local field enhancement in efficient nanolens: Cascade enhancement
Giant local fields in the minimum gap: Nanoscale localization of optical energy
Optical Electric Field
w=3.37 eV
500
30
100
w=3.25 eV
1500
100
500
0
w=0.77 eV
15
10
5
0
2/14/2005
Web: http://www.phy-astr.gsu.edu/stockman
E-mail: mstockman@gsu.edu
ITCP, Trieste, Italy
02/10/2005 23

Hot spots on gold

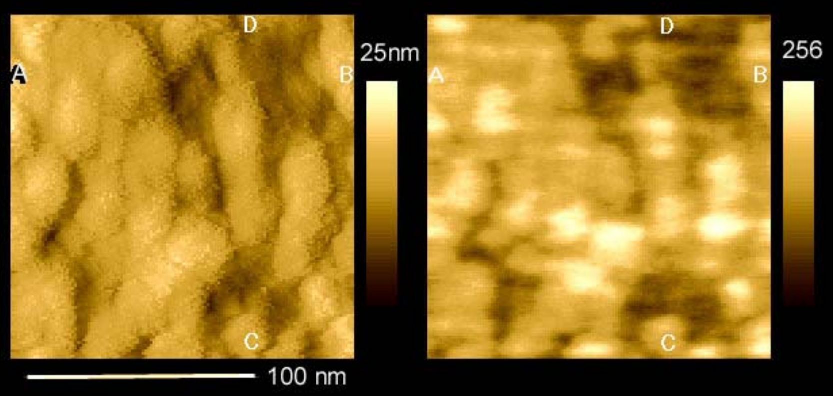

A.V.Bragas and O. E. Martínez, Optics Letters 25 (2000) pp.

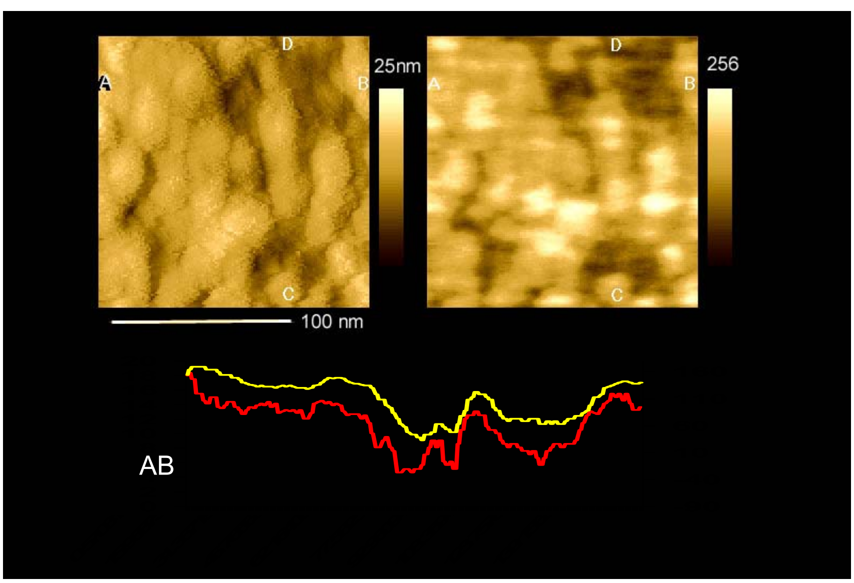

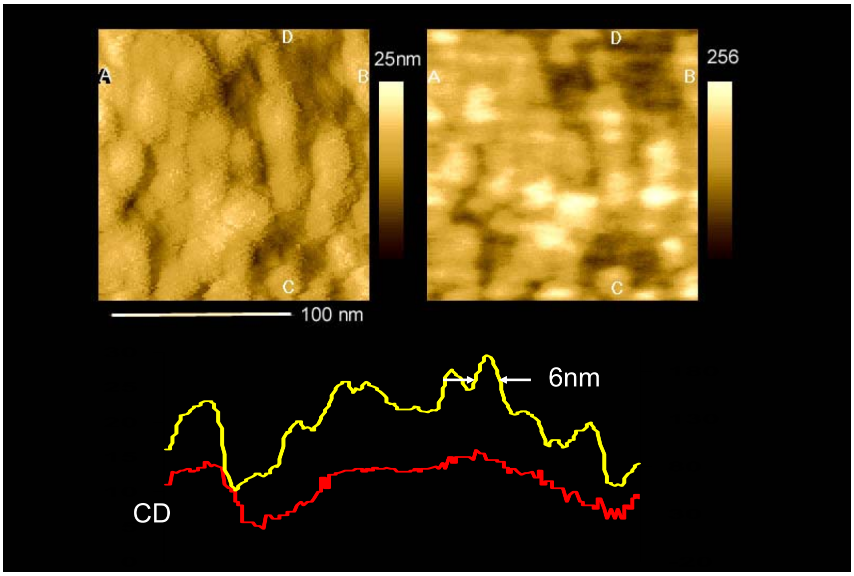

Enhancement: how large?

Laser field enhancement at the Scanning Tunneling Microscope junction measured by optical rectification", A.V. Bragas, S.M. Landi and O.E. Martínez, Appl. Phys. Lett. 72 (1998) pp. 2075-2077

Au-Pt
polarization: p

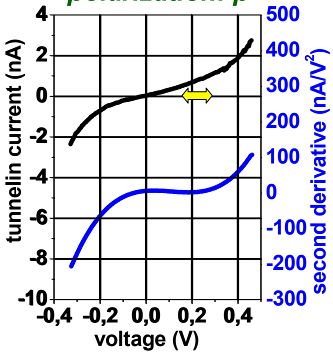

f=10kHz $> f_c$ *thermal*

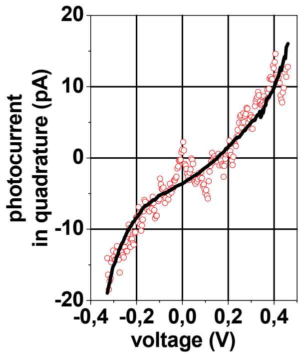

$$v_{Au-Pt} = \sqrt{2b}\ [V] = 13 \pm 0.4\ mV$$

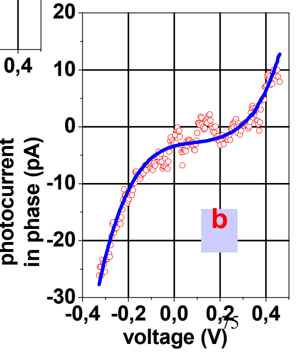

THE NUMBERS

$v_{Au-Pt} = 13 \pm 0.4\ mV$

$0.5nm < d < 1nm$

$7.4x10^7\ \frac{V}{m} < E_{loc} < 3.7x10^7\ \frac{V}{m}$

$E_{inc} \approx 4\ x\ 10^4\ V/m$

$300 \leq \gamma \leq 600$ $1000 \leq \gamma \leq 2000$

ADIABATIC NANOFOCUSING

Intensity of Local Fields at the Surface of Tapered Plasmonic Waveguide (Conic Silver Wire)

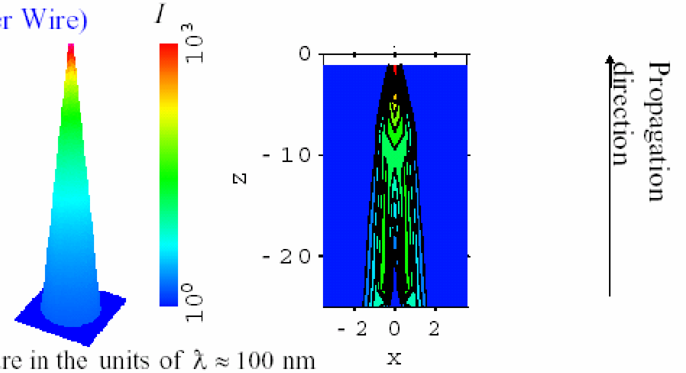

Coordinates are in the units of $\lambda \approx 100$ nm

M. I. Stockman, *Nanofocusing of Optical Energy in Tapered Plasmonic Waveguides*, Phys. Rev. Lett. **93**, 137404-1-4 (2004).

Estimated 50% energy delivered to the apex

Mode is dark: does not couple to radiation modes

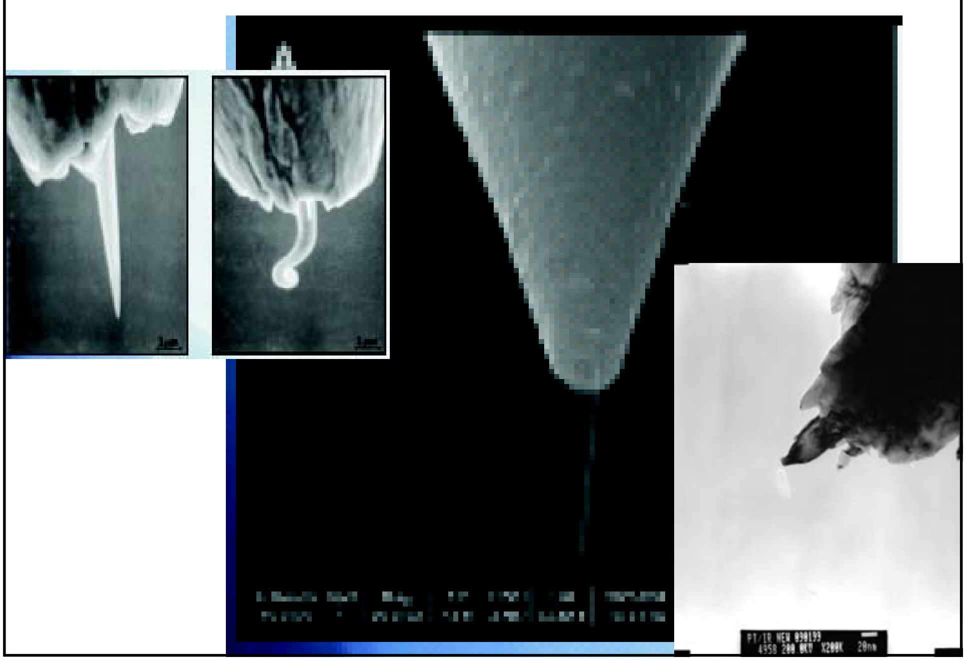

NEAR-FIELD RAMAN SCATTERING ?

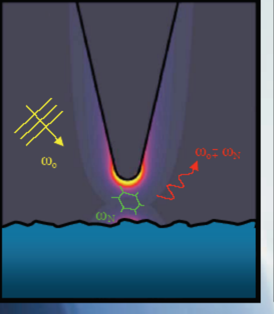

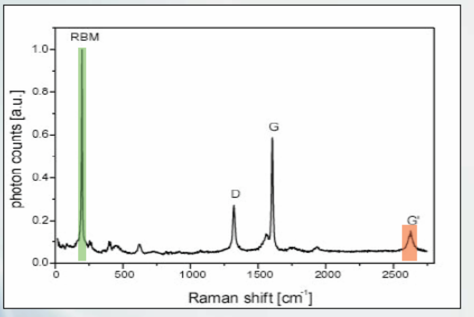

PRL **90**, 95503 (2003)

WHY RAMAN SCATTERING ?

Chemically specific ("fingerprint")

Intrinsic properties of molecular structures (no need for labels)

"No" photo-bleaching.

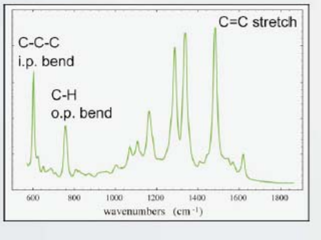

Raman signals can be locally enhanced by up to 10^{14} (SERS).

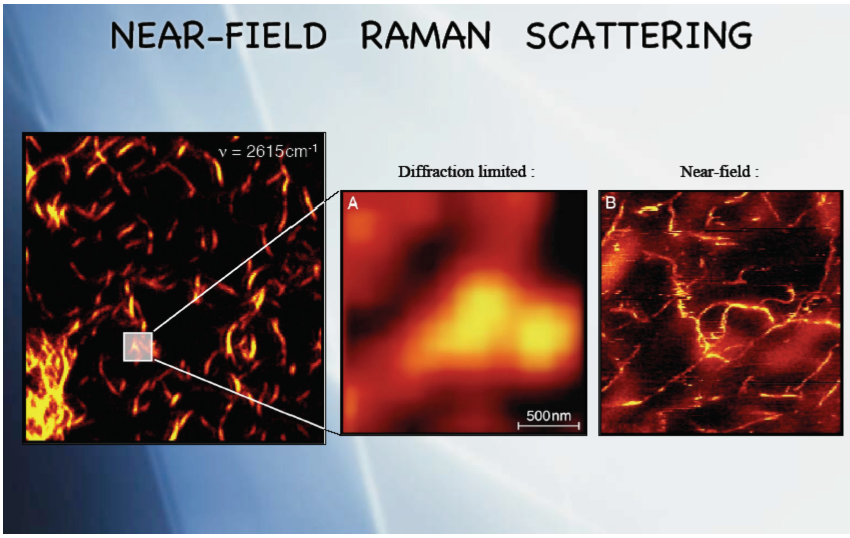
NEAR-FIELD RAMAN SCATTERING
ν = 2615cm-1
Diffraction limited :
Near-field :
A
B
500nm

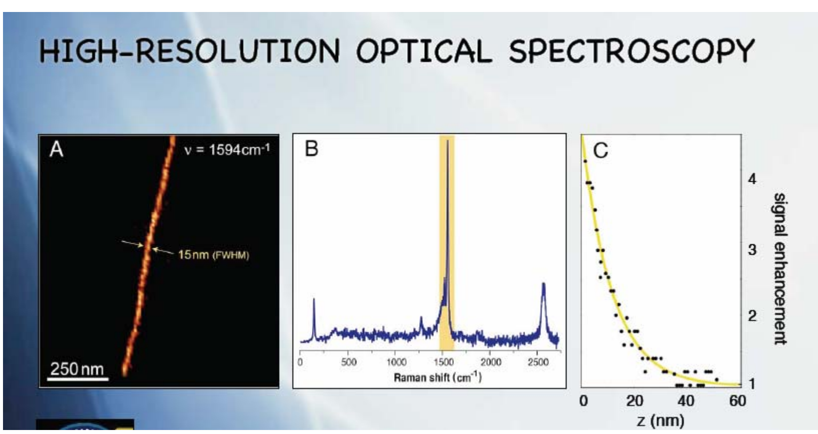
HIGH-RESOLUTION OPTICAL SPECTROSCOPY
A
ν = 1594cm-1
15nm (FWHM)
250 nm
B
0
500
1000
1500
2000
2500
Raman shift (cm-1)
C
4
3
2
1
signal enhancement
0
20
40
60
z (nm)

NEAR-FIELD SIGNAL ENHANCEMENT

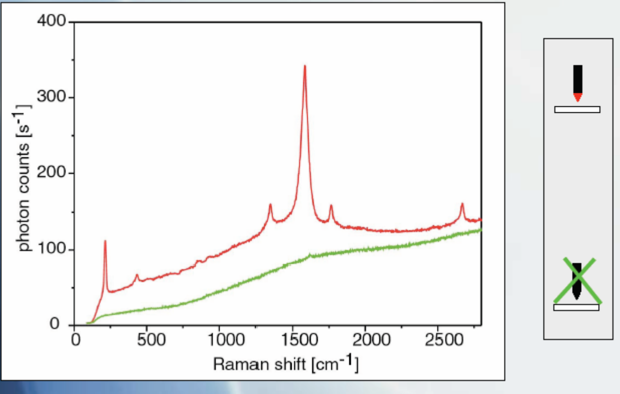

CHEMICAL SPECIFICITY

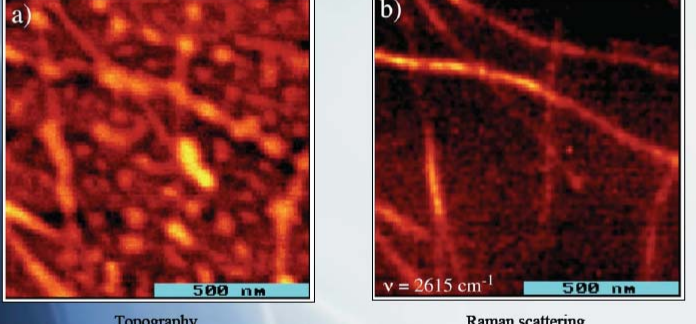

Topography

Raman scattering

PRL 90, 95503 (2003)

Near field approach

- **Are there limitations?**
- **The plasmonic highway**
- **Imaging**
- **New enhancement geometries**
- **Is imaging the only motivation?**

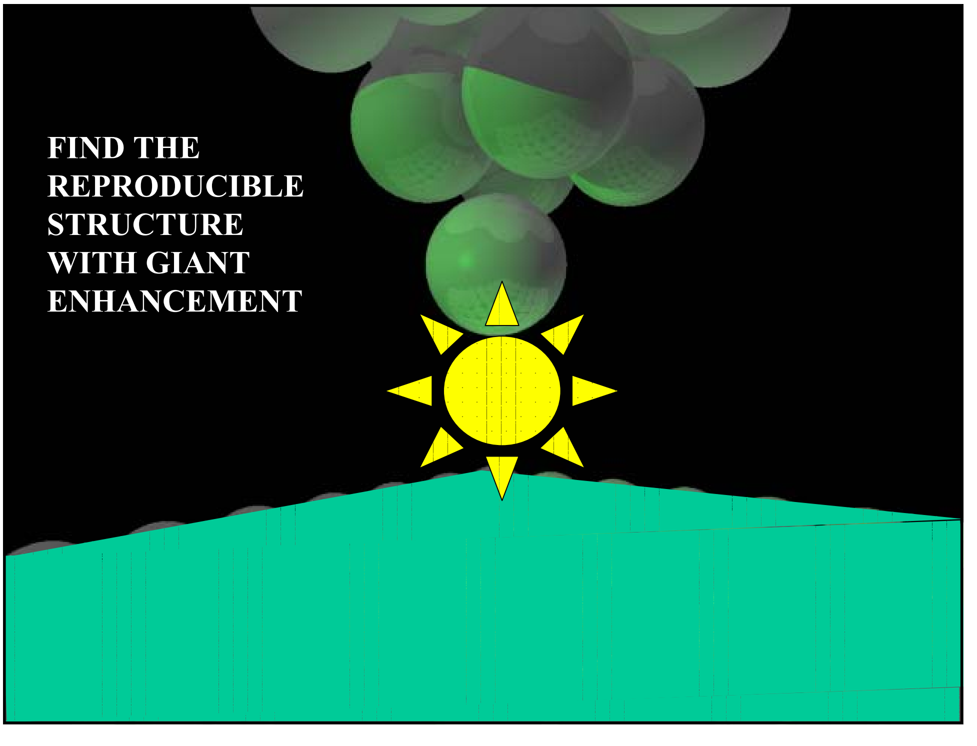

Other configurations

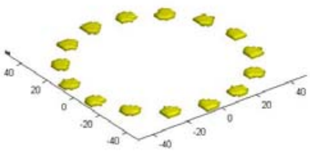

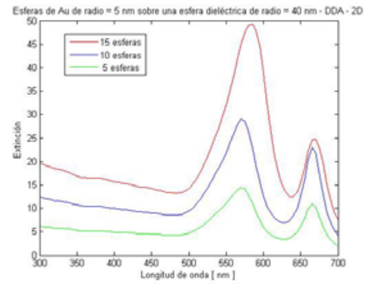

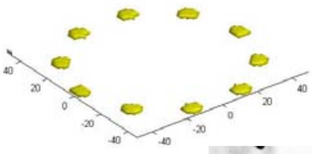

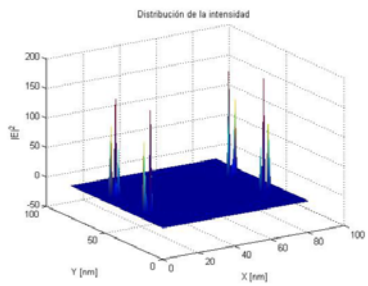

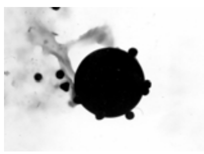

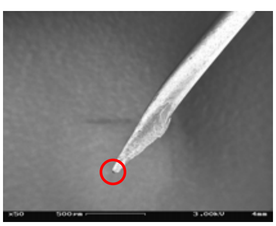

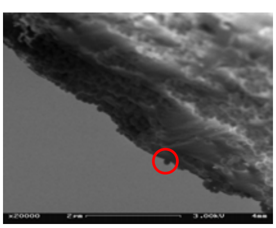

Tips

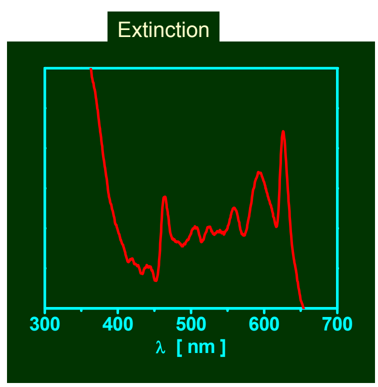

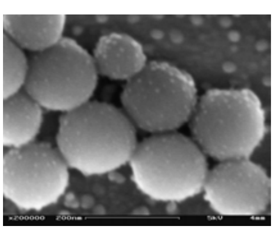

SiO_2 microspheres 170 nm.
Ag Nanoparticles 5 nm.

See Poster A. Scarpettini

Ag tips with Ag decorated SiO_2 particles

Sample: HOPG, Detection: 2Ω

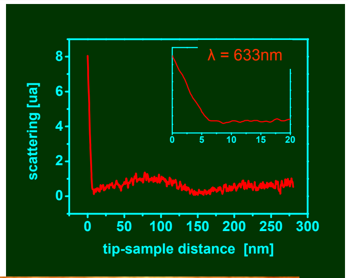

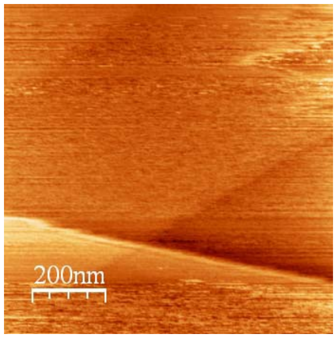

STM

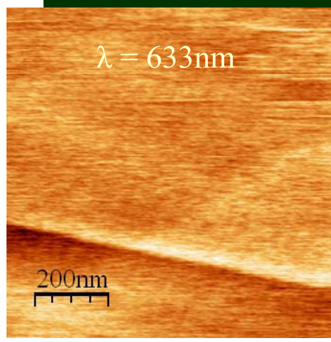

FESOM, 2Ω

Near field approach

- **Are there limitations?**
- **The plasmonic highway**
- **Imaging**
- **New enhancement geometries**
- **Is imaging the only motivation?**

Scattering: DISTANCE AND ORIENTATION

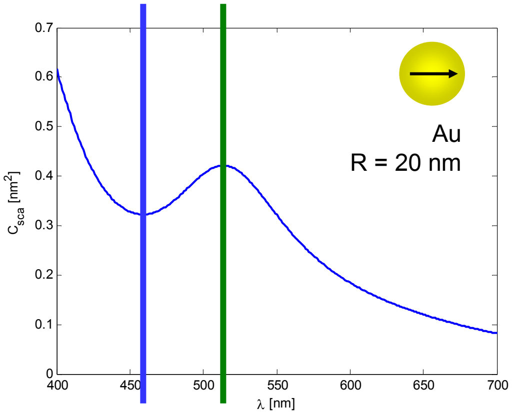

- Unlimited number of photons
- Unlimited rate of photons
- Biocompatible probe,
- Comercially available

EM Coupling

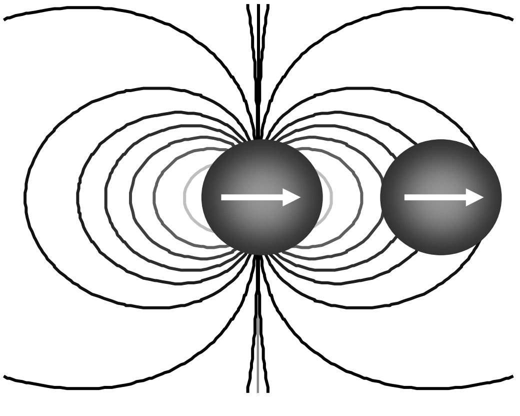

Numerical methods
Nanoparticle arrangements

MMIE technique

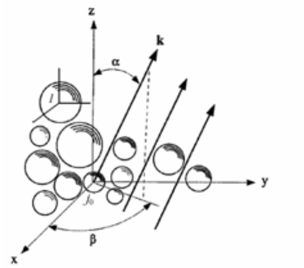

$$a^{j}_{mn} = a^{j}_{n}\left\{p^{j,j}_{mn} - \sum_{l\neq j}^{(1,L)}\sum_{\nu=1}^{\infty}\sum_{\mu=-\nu}^{\nu}\left[a^{l}_{\mu\nu}A^{\mu\nu}_{mn}(l,j) + b^{l}_{\mu\nu}B^{\mu\nu}_{mn}(l,j)\right]\right\}$$

$$b^{j}_{mn} = b^{j}_{n}\left\{q^{j,j}_{mn} - \sum_{l\neq j}^{(1,L)}\sum_{\nu=1}^{\infty}\sum_{\mu=-\nu}^{\nu}\left[a^{l}_{\mu\nu}B^{\mu\nu}_{mn}(l,j) + b^{l}_{\mu\nu}A^{\mu\nu}_{mn}(l,j)\right]\right\}$$

$$\mathbf{E}_s = \sum_{n=1}^{\infty}\sum_{m=-n}^{n} iE_{mn}\left[a_{mn}\mathbf{N}_{mn} + b_{mn}\mathbf{M}_{mn}\right]$$

$$a_{mn} = \sum_{l=1}^{L}\sum_{\nu=1}^{\infty}\sum_{\mu=-\nu}^{\nu}\left[a^{l}_{\mu\nu}A^{\mu\nu}_{mn}(l,j_0) + b^{l}_{\mu\nu}B^{\mu\nu}_{mn}(l,j_0)\right]$$

$$b_{mn} = \sum_{l=1}^{L}\sum_{\nu=1}^{\infty}\sum_{\mu=-\nu}^{\nu}\left[a^{l}_{\mu\nu}B^{\mu\nu}_{mn}(l,j_0) + b^{l}_{\mu\nu}A^{\mu\nu}_{mn}(l,j_0)\right]$$

(30:end)

DDA method

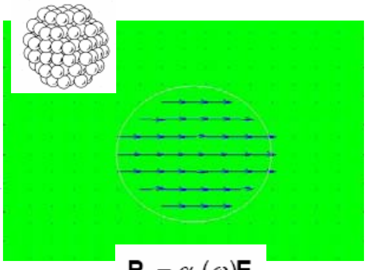

$$\mathbf{P}_j = \alpha_j(\omega)\mathbf{E}_j$$

$$E_j = E_{inc,j} - \sum_{k\neq j}^{N} A_{jk} P_k$$

$$\mathbf{A}_{jk} = \frac{\exp(ikr_{jk})}{r_{jk}} \times \left[k^2(\hat{\mathbf{r}}_{jk}\hat{\mathbf{r}}_{jk} - \mathbf{1}_3) + \frac{ikr_{jk} - 1}{r_{jk}^2}(\hat{\mathbf{r}}_{jk}\hat{\mathbf{r}}_{jk} - \mathbf{1}_3)\right] \quad j \neq k$$

Numerical methods
Nanoparticle arrangements

MMIE technique

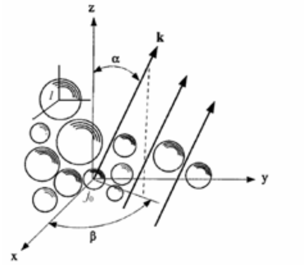

DDA method

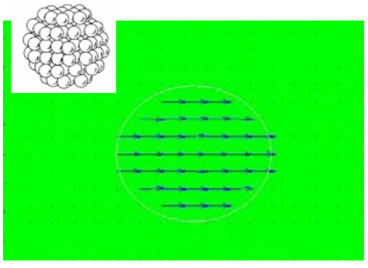

Detection

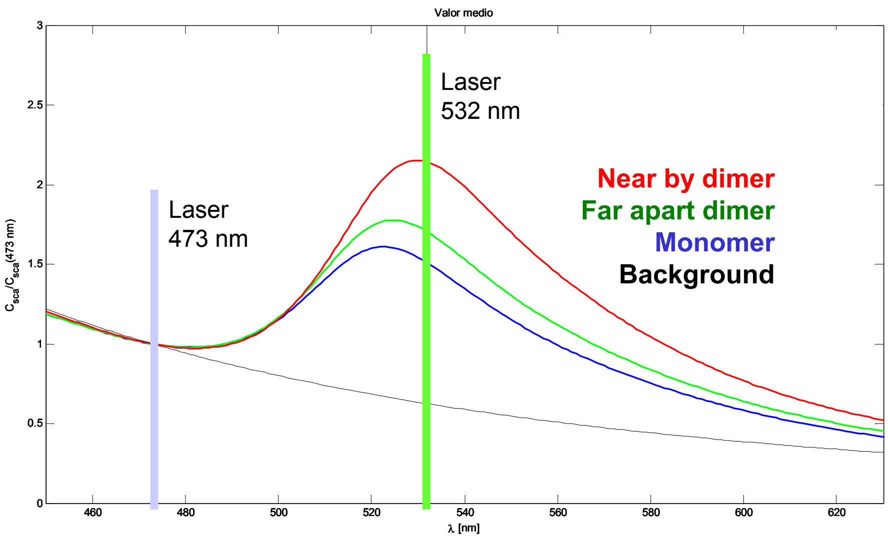

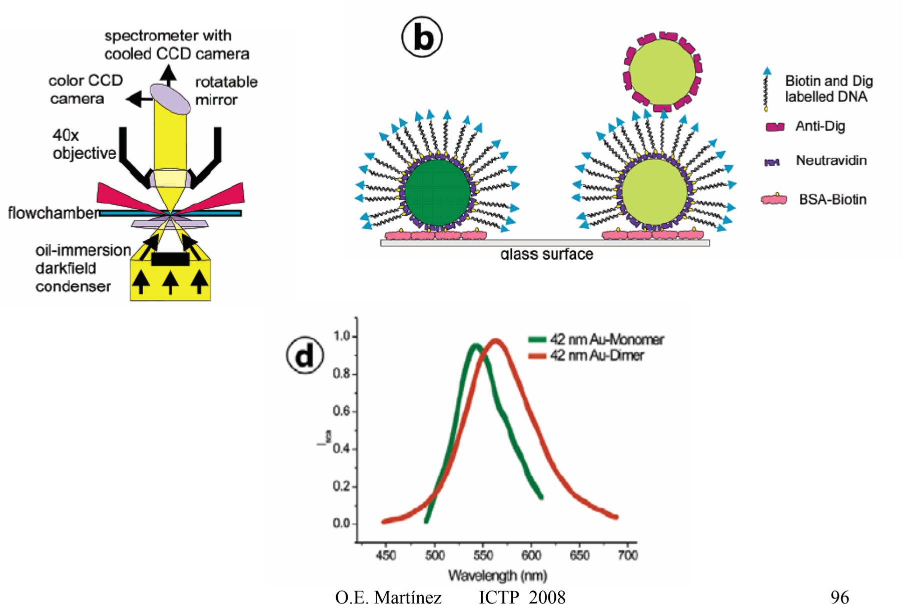

*Sonnichsen, C., Reinhard, B. M., et al. (2005). Nature Biotechnology **23**(6): 741-745.*

An average wavelength shift of approximately 1.24 nm is observed per DNA base pair.

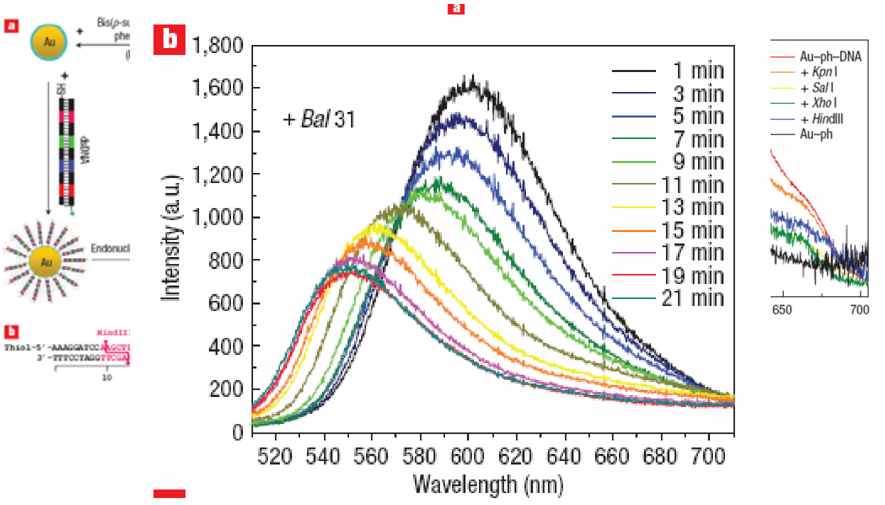

*Liu, G. L., Yin, Y., et al. (2006). Nature Nanotechnology **1**(1): 47-52.*

Basic concept

$$f = \frac{\vec{p}_{\text{coupled}}}{\vec{p}_{\text{non interacting}}}$$

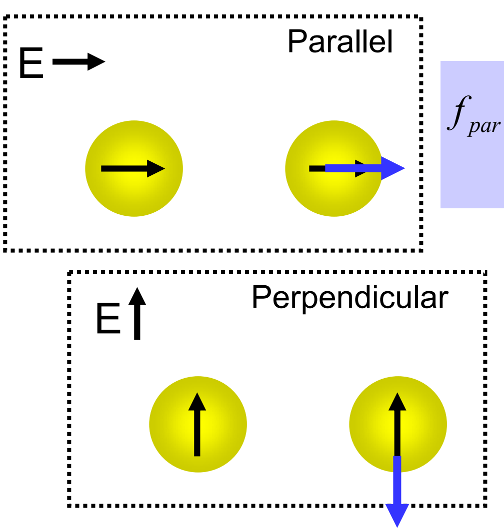

$$f_{par} = \frac{1}{1 - \dfrac{\alpha}{2d^3\pi}} > 1$$

r/d

$$f_{per} = \frac{2}{2 + \dfrac{\alpha}{2d^3\pi}} < 1$$

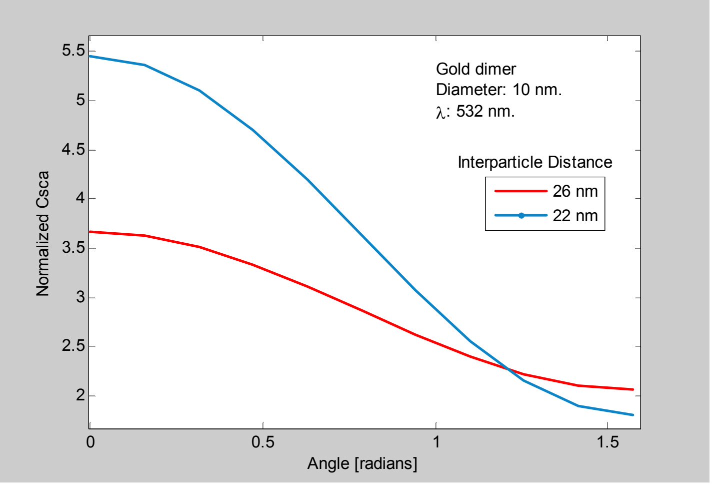
Gold dimer
Diameter: 10 nm.
λ: 532 nm.
Interparticle Distance
26 nm
22 nm
Normalized Csca
Angle [radians]

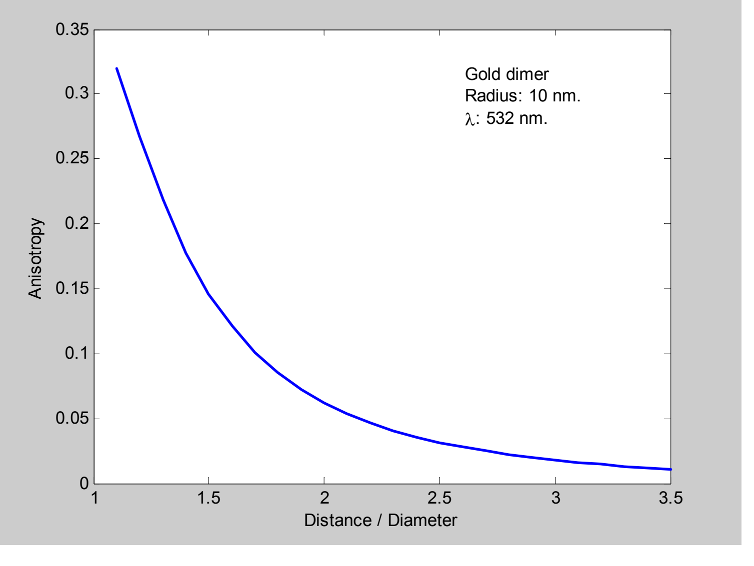
Gold dimer
Radius: 10 nm.
λ: 532 nm.
Anisotropy
Distance / Diameter

Beyond the dipolar approximation

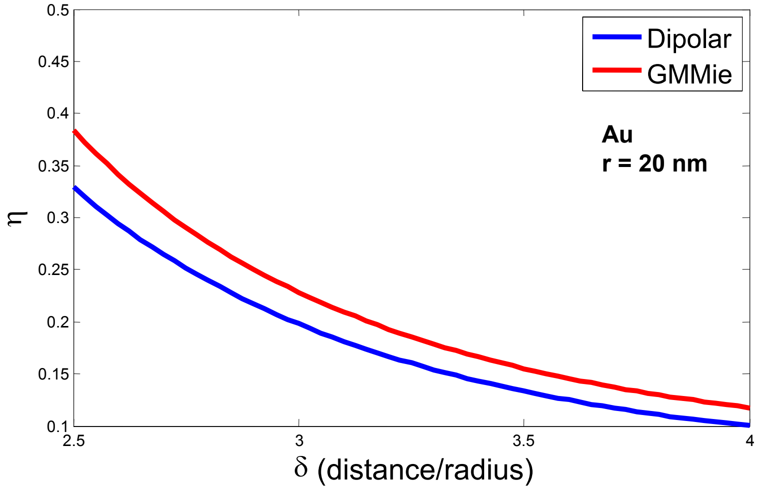

GMMie: Multiparticle expansion based on Mie theory (solved numerically)

Typical TIR image

λ_{exc} = 532 nm
50x50μm
100 ms

1 sequence
= 2 seg

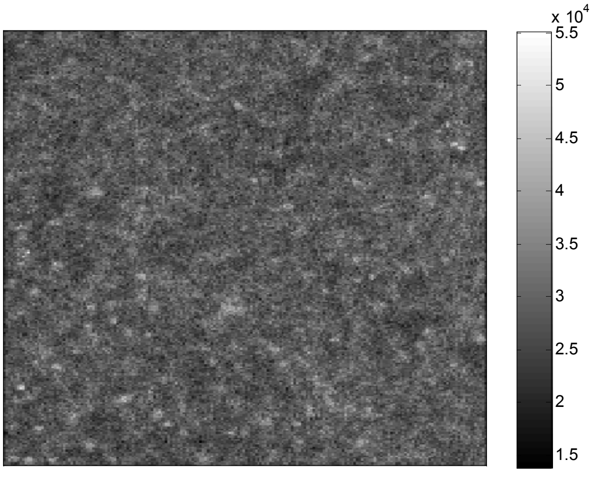

Results

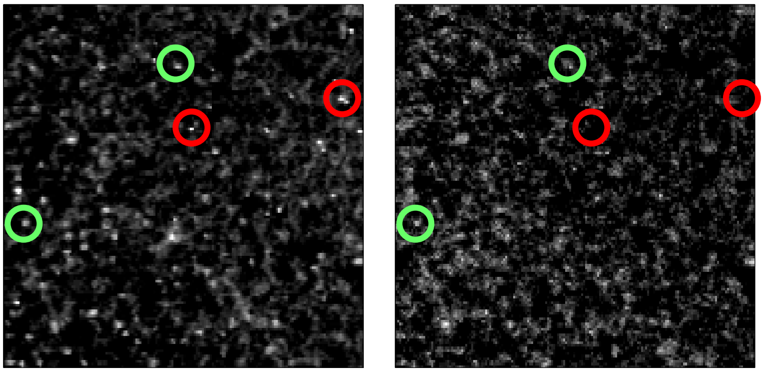

532

532/473

With only one color you get about twice the number of points (false positives and negatives)

50x50μm

Fit of 30 images

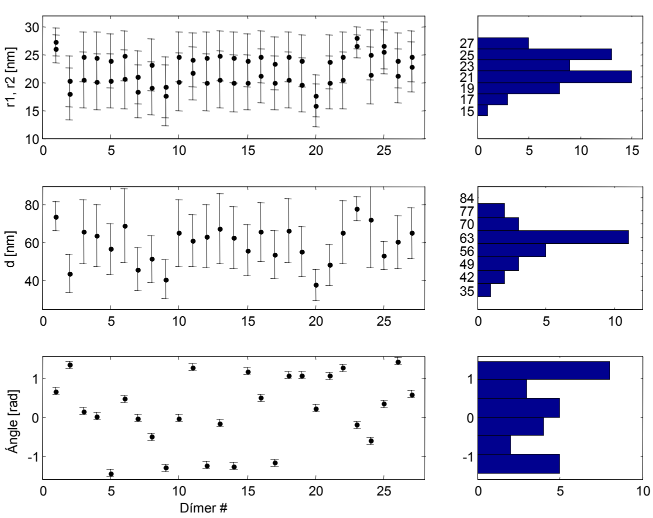

Results

Dímer # 18
R_1 ~ 20 nm
R_2 ~ 24 nm
D ~ 67 nm
ε ~ 59°

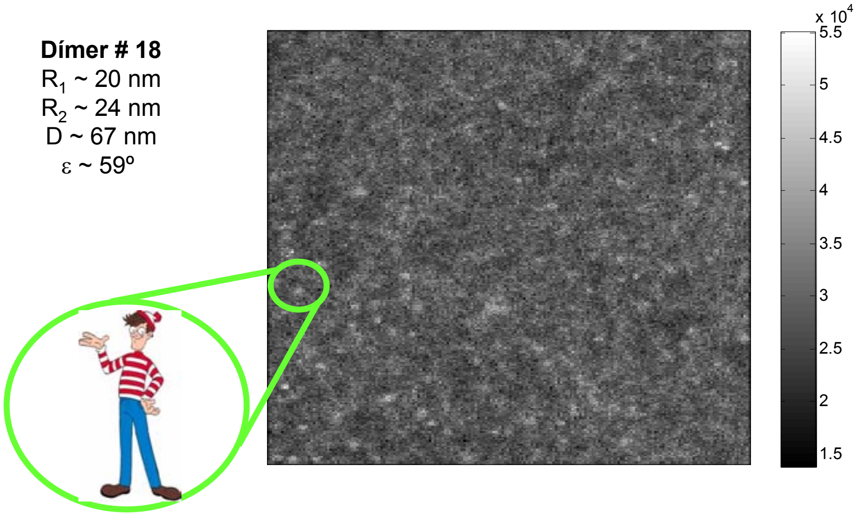

Fluorescence correlation spectroscopy at reduced volumes

- Brief introduction to FCS. Why reduced volumes?
- See poster Laura Estrada
- Se talk Prof. Lenne

FCS

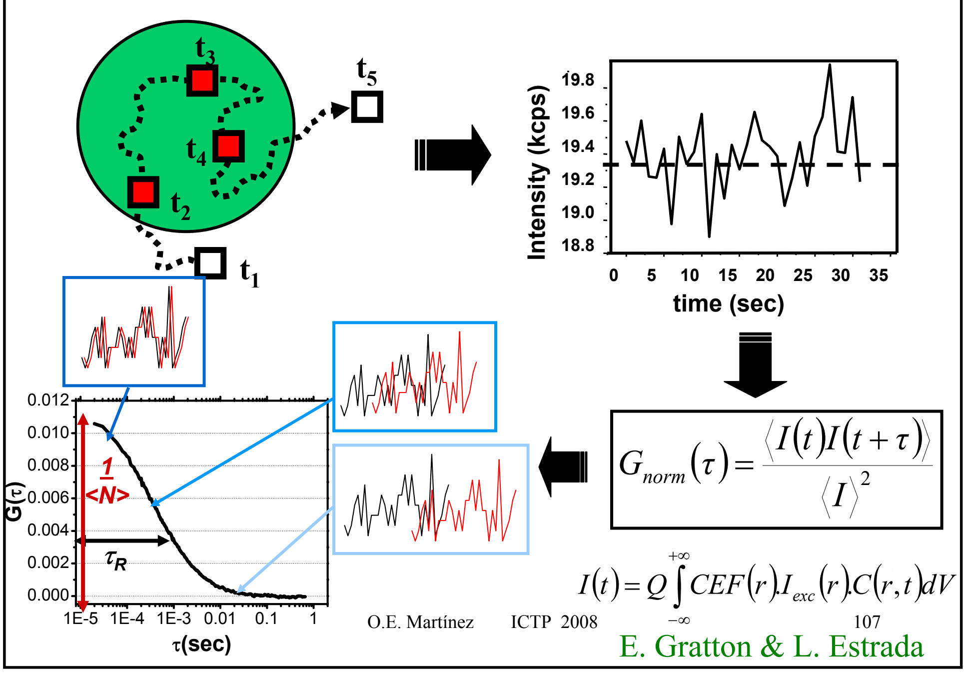

$$G_{norm}(\tau) = \frac{\langle I(t)I(t+\tau)\rangle}{\langle I\rangle^2}$$

$$I(t) = Q\int_{-\infty}^{+\infty} CEF(r).I_{exc}(r).C(r,t)\,dV$$

E. Gratton & L. Estrada

Outline

1. Introduction and motivations
2. Localization vs. resolution
3. Nonlinear approach
4. Near field approach
5. Newcomers
   - Short wavelength sources
   - Superlenses

Capillary discharge laser – 46.9 nm

• High fluence: mW average power

• High monochromaticity

• High spatial coherence

•Rep rate 4 Hz
•High energy per pulse [0.8 mJ]
•High monochromaticity
•Average power [3 mW]

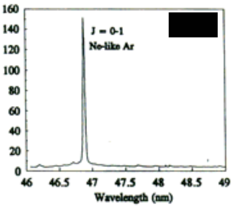

J.J. Rocca, el al. Phys. Rev. Lett. **73**, 2192 (1994).

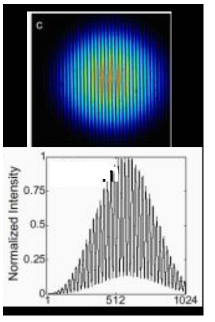

Y. Liu, et al. Phys. Rev. A, **63**, 033802 (2001).

Interferomeric lithography at SXR wavelengths

Source: 46.9 nm discharge pumped table top laser
Compact tool
Printing different motifs on PMMA and HSQ

M. C. Marconi, P. Wachulak, M. Capeluto, D. Patel, C. S. Menoni, J. J. Rocca,

NSF Engineering Research Center for Extreme Ultraviolet Science and Technology
and
Department of Electrical and Computer Engineering, Colorado State University
Fort Collins, CO 80523, USA

Table top nano-patterning tool

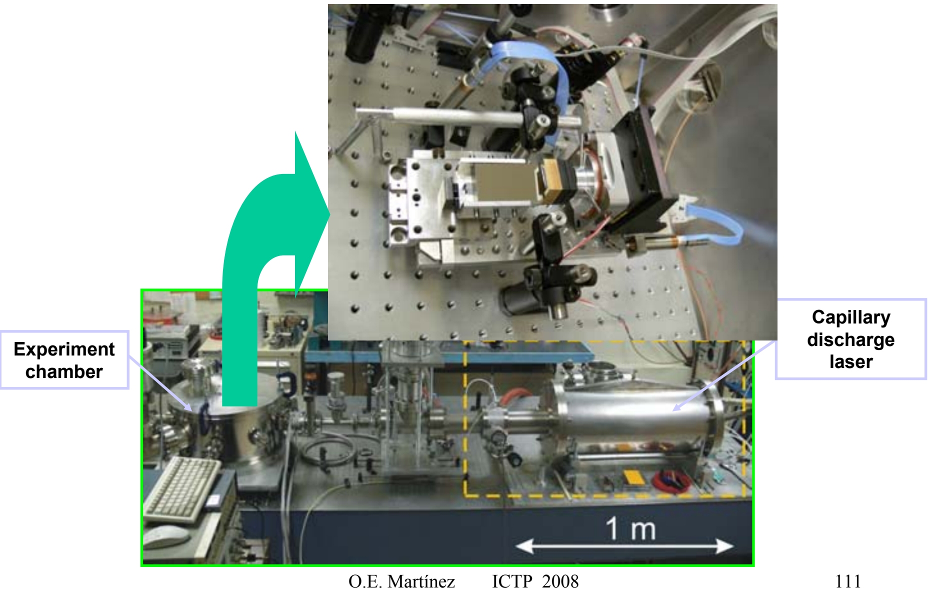

Table top Nanopatterning

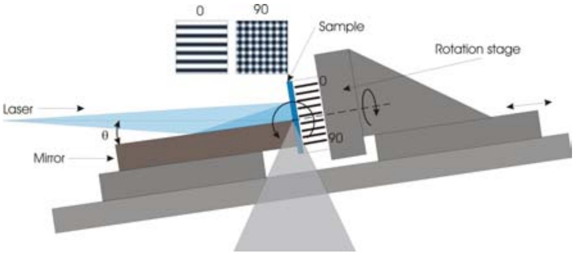

Double exposure set up with a Lloyd's mirror

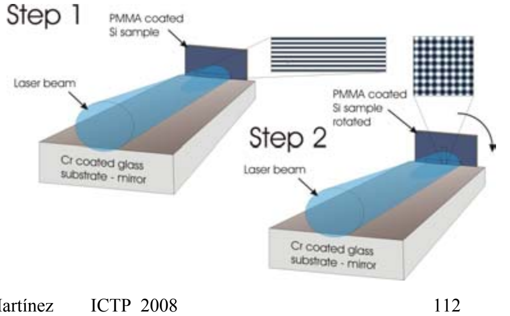

Two successive exposures allows printing arrays of nanometer size features

Printing area: coherence limitations

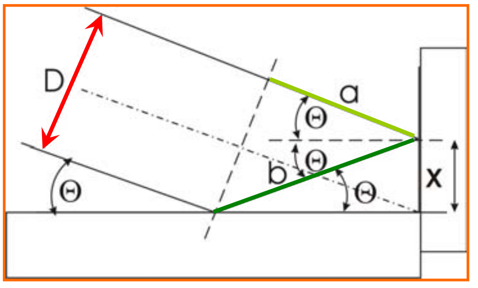

• Spatial coherence:

Requirement: $D \le 2R_c$

$$x = \frac{R_c}{\cos(\Theta)}$$

• Temporal coherence:

Requirement: $b - a \le l_c$

$$x = \frac{l_c}{2\sin(\Theta)}$$

Radius of coherence:

$R_c \sim 0.5mm$

Coherence length:

$$l_c = \frac{\lambda^2}{\Delta\lambda} \approx 470\mu m$$

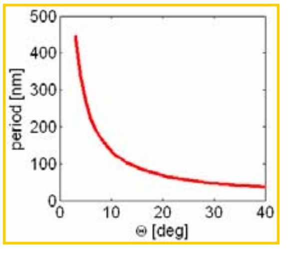

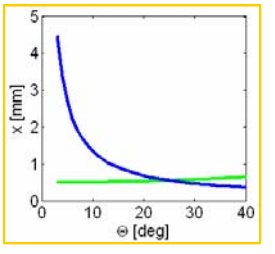

Table top Nanopatterning PMMA: large areas

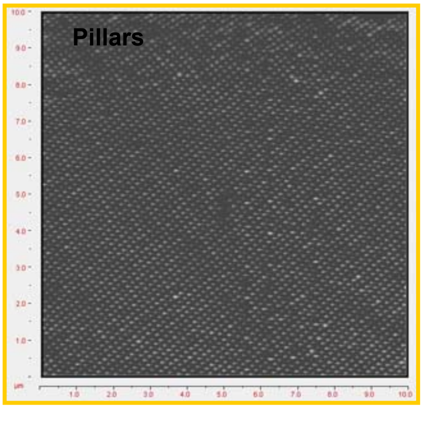

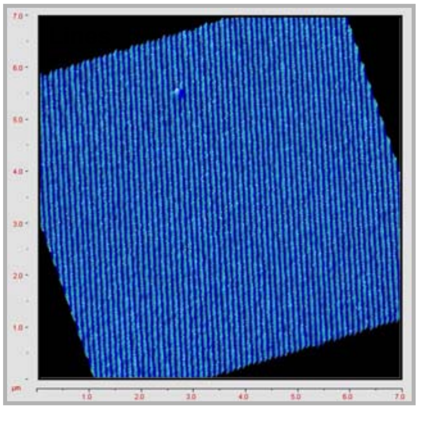

*Period **140nm**,*
*pillars FWHM **~70nm***
Scan size 10x10µm²

*Period **95nm**,*
*lines FWHM **~47nm***
Scan size 7x7µm²

Patterning areas in excess 500 x 500 µm^2

10 x 10 µm^2

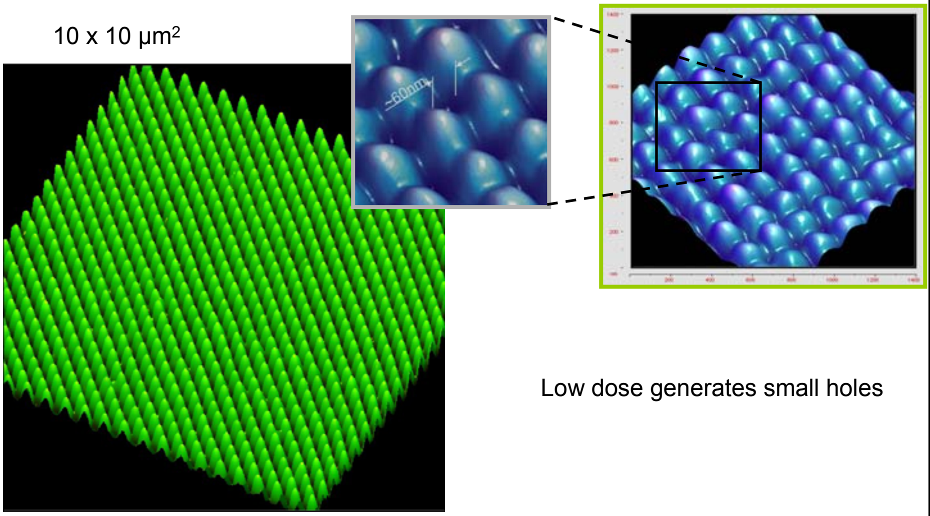

Low dose generates small holes

Table top Nanopatterning PMMA: oval nanodots

Different rotation angles allows printing different motifs

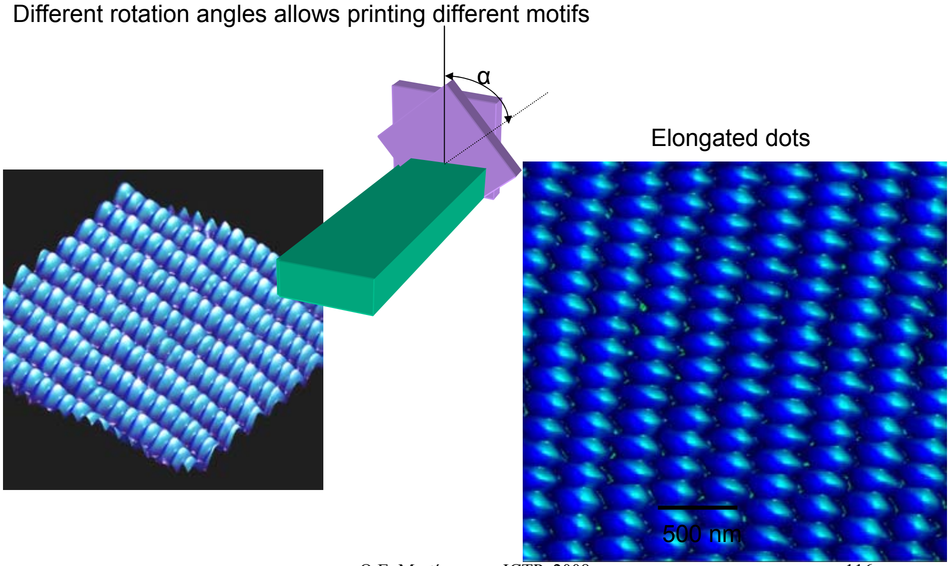

Table top Nanopatterning PMMA: High dose

Dose: 32 mJ cm^{-2}

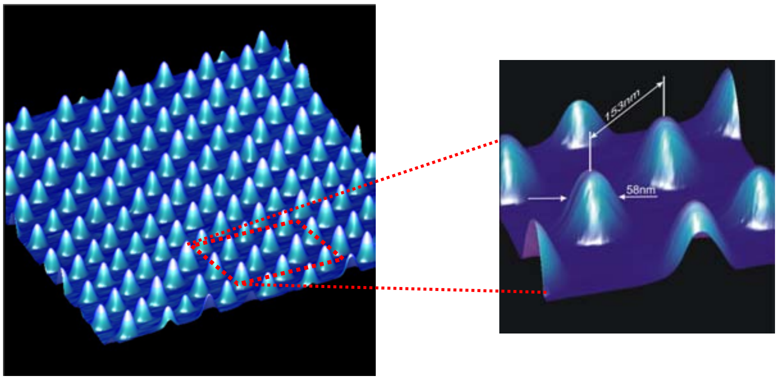

Other applications: Full field zone plate microscope at λ=46.9 nm can image the surface of semiconductor chips.

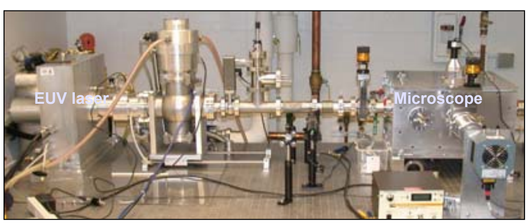

TRANSMISSION MODE

20 sec exposure EUV image of 70 nm half period dense lines - Δr =70 nm

Spatial resolution <70 nm

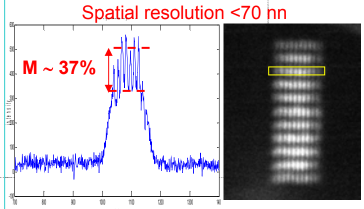

REFLECTION MODE

20 sec exposure EUV images of the surface of a semiconductor chip - Δr=200 nm

Spatial resolution: 150 nm

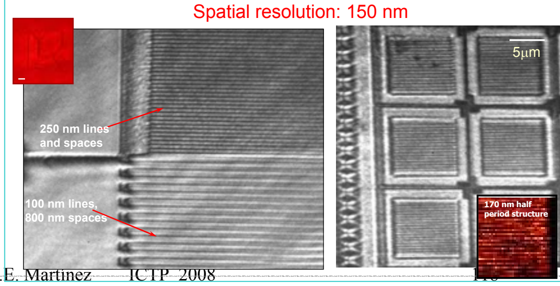

Holographic Nano-Imaging Realized with Compact Extreme Ultraviolet Lasers

M. C. Marconi, P. Wachulak, R. A. Bartels,
C. S. Menoni and J. J. Rocca

NSF ERC for Extreme Ultraviolet Science & Technology
and Department of Electrical and Computer Engineering,
Colorado State University
wachulak@lamar.colostate.edu

EUV Holography

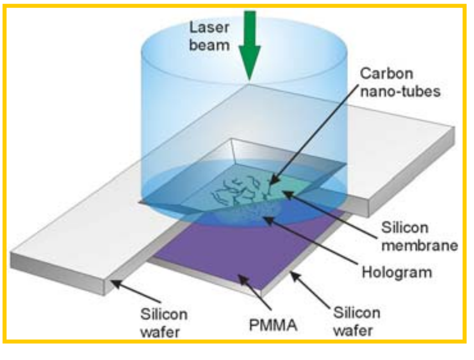

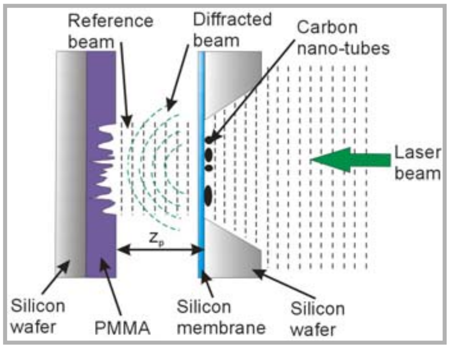

Object :

Multi-Wall Carbon Nanotubes (manufacturer specs.):

- Outer Diameter **50-80nm**
- Length 10-20μm
- Purity > 95%
- Ash <1.5wt%

www.cheaptubesinc.com

Experimental details:

- z_p ~2.5 - 4 μm
- Laser-object distance z_s =75cm
- Laser shots = 150
- Dose = 53mJ/cm^2

50-80 nm CNT

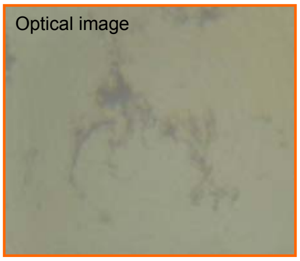

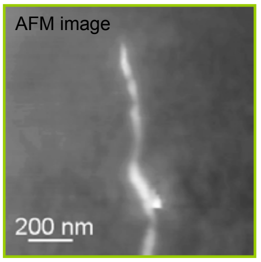

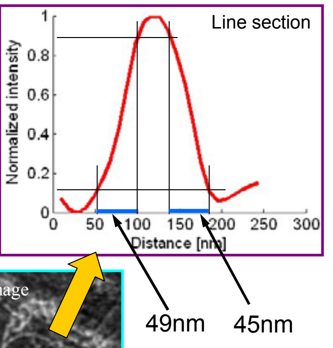

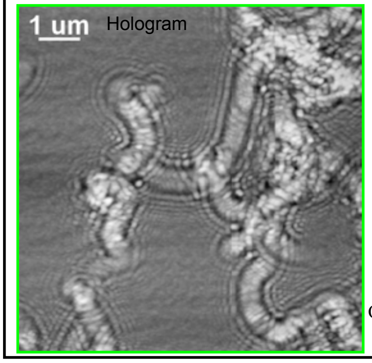

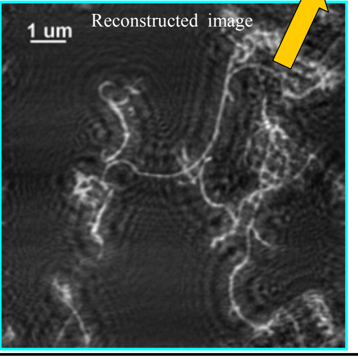

- z_p = **2.6 μm**
- pixel size = **9.7nm**
- scan size **10x10 μm²**

30-50 nm CNT

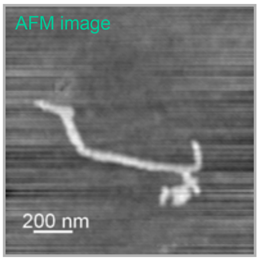

Hard to obtain good quality image with AFM

Carbon nano-tubes move as they are scan with the AFM tip

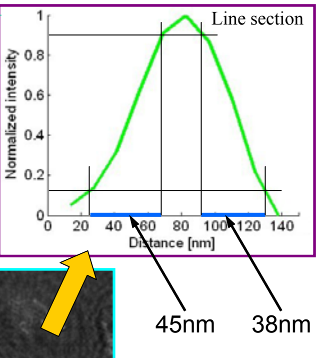

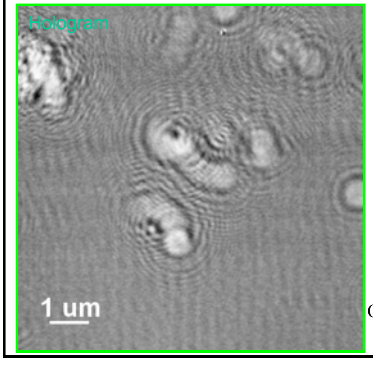

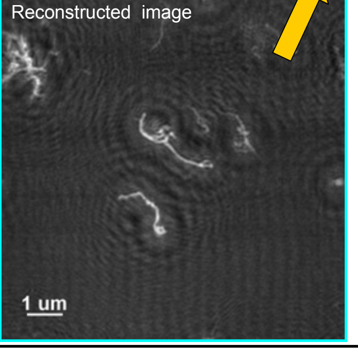

- z_p = **3.94 μm**
- pixel size = **9.7nm**

Resolution: EUV laser coherence parameters

Coherence limitations:

- transversal coherence

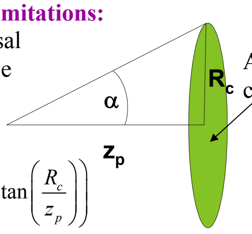

$$NA_{\max} = \sin\left(a\tan\left(\frac{R_c}{z_p}\right)\right)$$

- longitudinal coherence

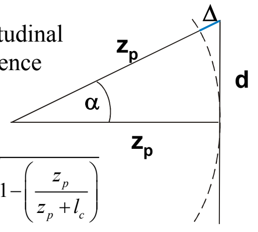

$$NA_{\max} = \sqrt{1-\left(\frac{z_p}{z_p+l_c}\right)}$$

Table with resolutions for…	Transversal coherence	Longitudinal coherence	Experimental resolution
z_p = 4 mm	*337.8 nm*	*64.1 nm*	*381 nm*
z_p = 120 μm	*30.4 nm*	*29.2 nm*	*164 nm*
z_p = ~2.5 μm - 4 μm	*28.6 nm*	*28.6 nm*	*~ 48 nm*

$$\boxed{\delta = \frac{0.61\lambda}{NA_{\max}}}$$

Rayleigh criterion for resolution

Hologram scanning limitations:

$$\boxed{N_{total} = \left(N_{samples}/line\right)^2 \sim \left(\frac{\lambda \cdot z_p}{\delta^2}\right)^2}$$

Real limitation to the resolution.

Conclusions

- ***sub-50 nm*** *(wavelength) resolution in the recording and reconstruction of a holographic image obtained in the Gabor's geometry with a table top EUV laser was demonstrated,*

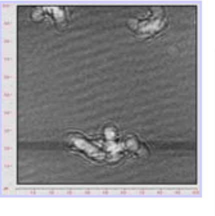

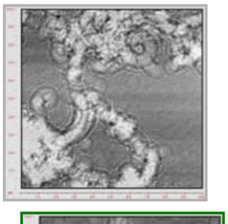

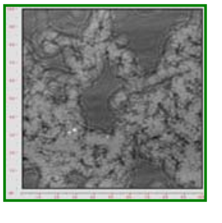

- *to determine the optimum reconstruction parameters and assess the spatial resolution of the holographic recording we used a* ***correlation analysis****,*

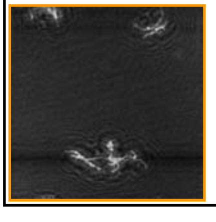

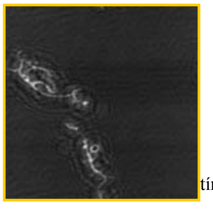

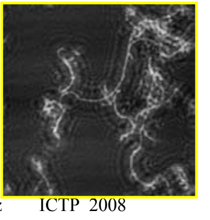

Lens-less imaging: sub 100nm

•*SXR table-top lensless imaging with **sub 100nm** resolution*

Richard Sandberg, Ariel Paul, Daisy Raymondson, Margaret Murnane, Henry Kapteyn, Changyong Song, Janwei Miao, Przemyslaw Wachulak, Mario Marconi, Carmen Menoni, Jorge Rocca, Anne Sakdinawat

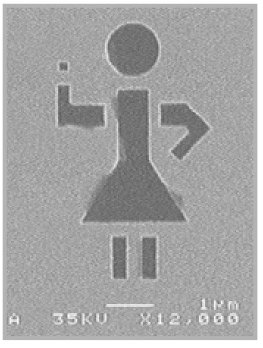

object

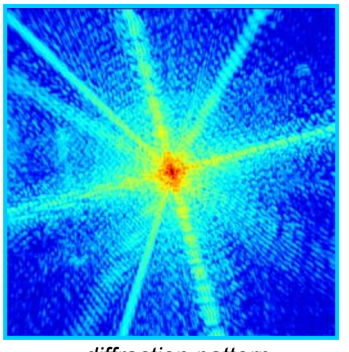

diffraction pattern

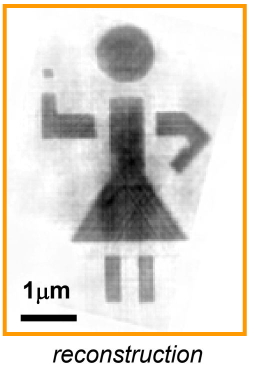

reconstruction

Other SXR sources to come

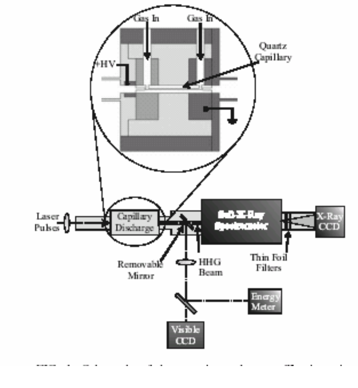

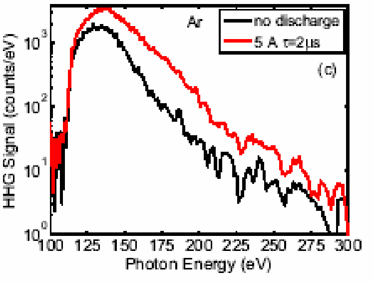

High-order harmonic spectra on a log scale with solid red and without dashed black the discharge showing an extension of the HHG cutoff to photon energies of above275 eV in 6 Torr of Ar with 11 mJ laser pulses.

B. A. Reagan, et al PHYSICAL REVIEW A **76**, 013816 2007

Enhanced high-order harmonic generation from Xe, Kr, and Ar in a capillary discharge

Outline

1. Introduction and motivations
2. Localization vs. resolution
3. Nonlinear approach
4. Near field approach
5. Newcomers
   – Short wavelength sources
   – Superlenses

Metamaterials and Negative Refractive Index

D. R. Smith, J. B. Pendry, M. C. K. Wiltshire

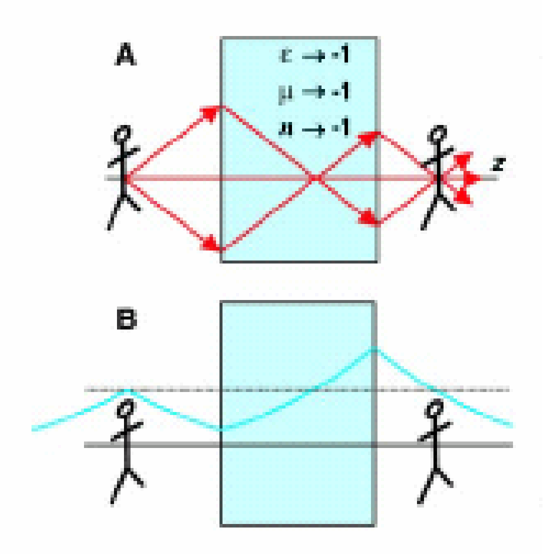

PLASMONS

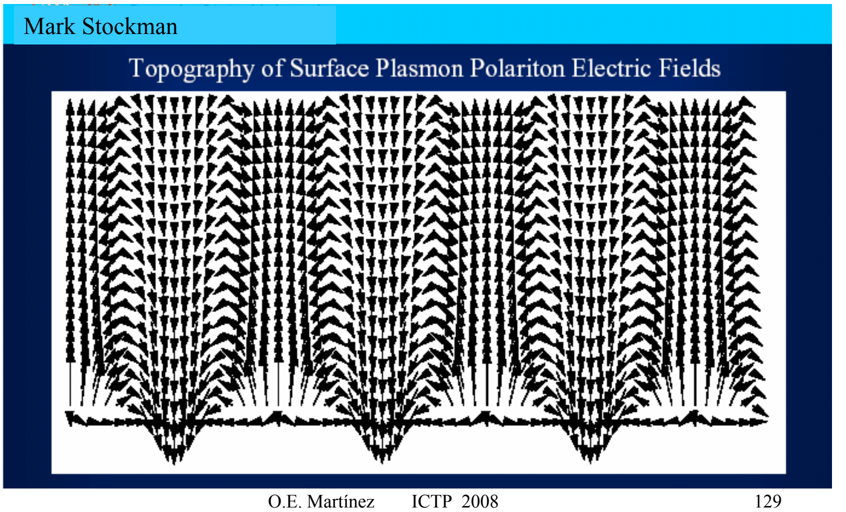

If $\varepsilon = -1$ and $\mu = -1$,

then $n = -1$,

the transmission coefficient for each Fourier component results

$$T = \exp\left(-i\sqrt{\omega^2 c^{-2} - k_x^2 - k_y^2}\, d \right)$$

The negative phase of the transmission coefficient is a result of the negative refractive index. Thus traversing a thickness *d* of 1 $n =$. material cancels the phase acquired in traversing an equal thickness of vacuum. Hence the focussing effect of the new medium.

What happens to the waves with very large *k//*?

$$\lim_{\substack{\varepsilon\to-1\\ \mu\to-1}} T_P = \lim_{\substack{\varepsilon\to-1\\ \mu\to-1}} \frac{2\varepsilon k_z}{\varepsilon k_z + k_z'} \frac{2k_z'}{k_z' + \varepsilon k_z} \frac{\exp\left(ik_z d\right)}{1-\left(\dfrac{k_z' - \varepsilon k_z}{k_z' + \varepsilon k_z}\right)^2 \exp\left(2ik_z' d\right)}$$

$$= \exp\left(-ik_z d\right)$$

If we want to use visible radiation to make an image of a very small object which is much smaller than the wavelength of light, but that the distance between object and image is also very small.

$$k_{||} >> \omega c_0^{-1}$$

Then:

$$k_z = i\sqrt{k_x^2 + k_y^2 - \omega^2 c^{-2}} \approx i\sqrt{k_x^2 + k_y^2}$$

and

$$k_z' = i\sqrt{k_x^2 + k_y^2 - \varepsilon\mu\omega^2 c^{-2}} \approx i\sqrt{k_x^2 + k_y^2}$$

hence

$$\lim_{k_{\|}>>\omega c_0^{-1}} T_P = \lim_{k_{\|}>>\omega c_0^{-1}} \frac{2\varepsilon k_z}{\varepsilon k_z + k_z^{'}} \frac{2k_z^{'}}{k_z^{'} + \varepsilon k_z} \frac{\exp\left(ik_z^{'} d\right)}{1-\left(\frac{k_z^{'}-\varepsilon k_z}{k_z^{'}+\varepsilon k_z}\right)^2 \exp\left(2ik_z^{'} d\right)}$$

$$= \frac{4\varepsilon \exp\left(-k_{\|} d\right)}{(1+\varepsilon)^2 - (1-\varepsilon)^2 \exp\left(-2k_{\|} d\right)}$$

Hence the transmission coefficient for P polarised waves of very short wavelength depends only on ε and not at all on μ. With ε=-1,

$$\lim_{\substack{\varepsilon\to -1 \\ k_{\|}>>\omega c_0^{-1}}} T_P = \lim_{\varepsilon\to -1} \frac{4\varepsilon \exp\left(-k_{\|} d\right)}{(1+\varepsilon)^2 - (1-\varepsilon)^2 \exp\left(-2k_{\|} d\right)} = \exp\left(+k_{\|} d\right)$$

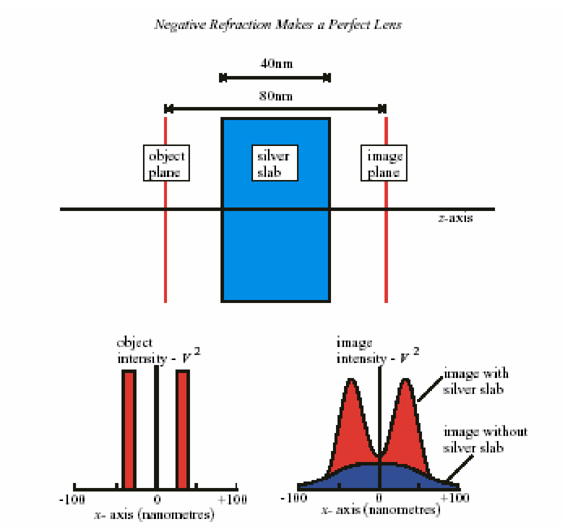

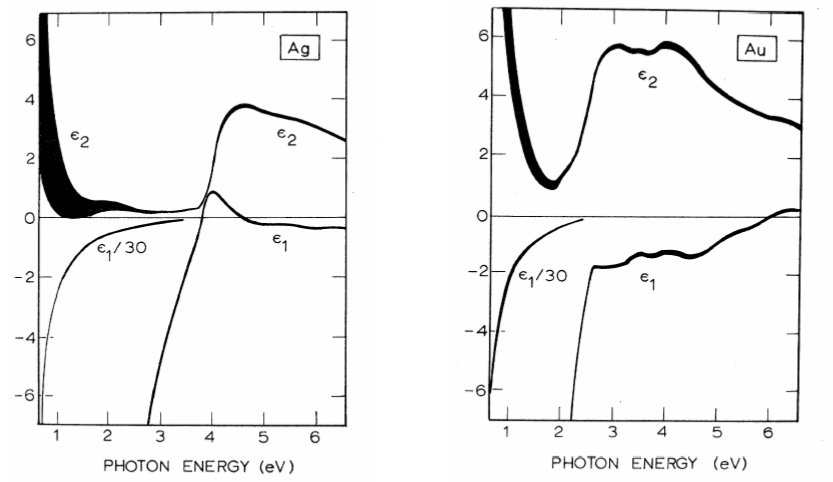

PHYSICAL REVIEW B VOLUME 6, NUMBER 12 15 DECEMBER 1972

Optical Constants of the Noble Metals

P. B. Johnson and R. W. Christy

A. Larkin and M. I. Stockman, *Imperfect Perfect Lens*, Nano Lett. (2005).

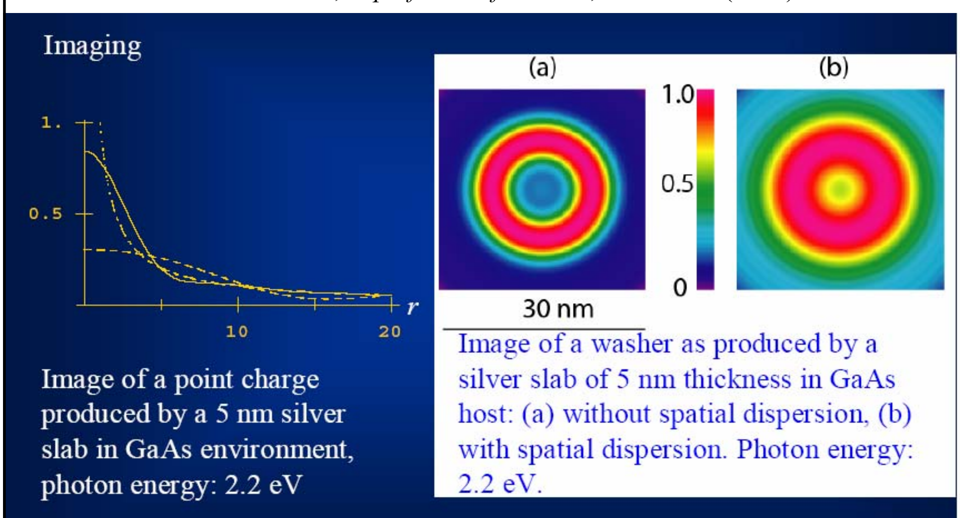

A. Larkin and M. I. Stockman, *Imperfect Perfect Lens*, Nano Lett. (2005).

At small distances a, interactions transfer large momentum $p \sim \dfrac{\hbar}{a}$

or wave vector $k \sim \dfrac{1}{a}$

For large enough k, $\dfrac{\omega}{k} \sim \omega a \leq v_F \sim 10^8 \dfrac{\text{cm}}{\text{s}}$ *interacting* electron system exhibits strong spatial dispersion and Landau damping . These effects are described by Klimontovich-Silin-Lindhart (RPA) formula

$$\varepsilon(\omega, k) = 1 + \frac{3\Omega_e^2}{k^2 v_F^2}\left[1 - \frac{\omega}{2kv_F}\ln\frac{\omega + kv_F}{\omega - kv_F}\right]$$

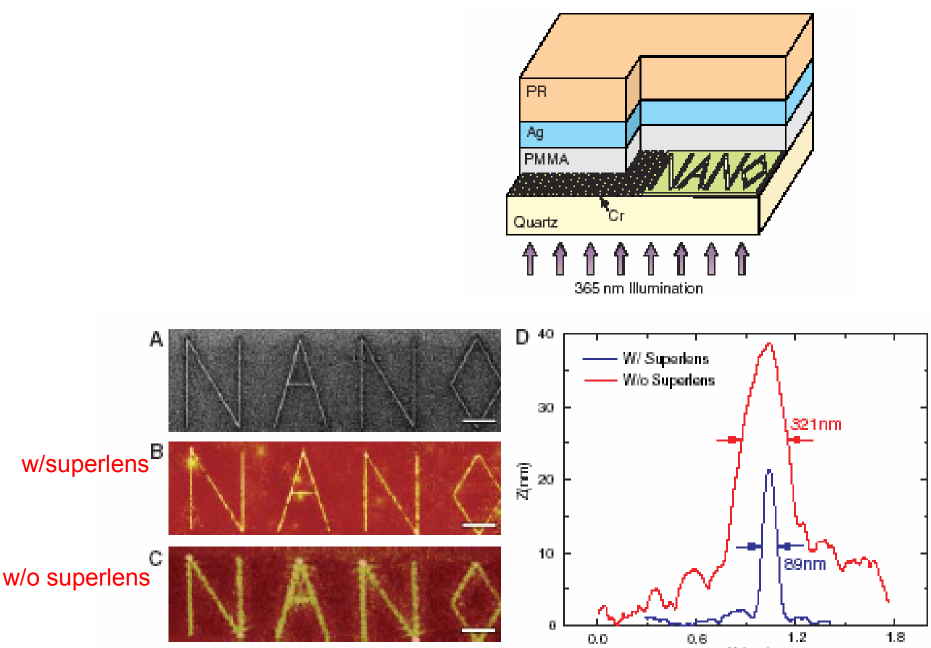

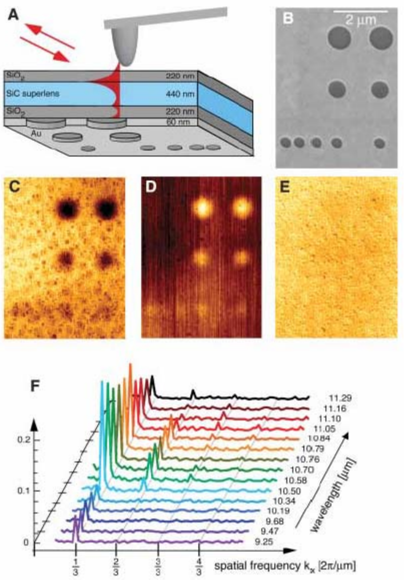

Near-Field Microscopy Through a 880nm SiC Superlens

(A) Experimental setup. (B) Scanning electron micrograph (mirrored) of the object plane, showing holes in a 60-nm-thick Au film. (C) Infrared amplitude in the image plane at λ=10.85 µm where superlensing is expected. (D) Infrared phase contrast (λ= 11.03 µm). (E) Control image showing infrared amplitude at λ= 9.25 µm (no superlensing). (F) Fourier tranforms of line scans taken from amplitude images of a grating (~3 µm period, averaged over 26 scan lines), normalized to unity for zero frequency. High spatial frequencies (up to the grating's fourth harmonic) are imaged by the superlens/s-SNOM system around λ= 10.84 µm wavelength.

Thomas Taubner, Dmitriy Korobkin, Yaroslav Urzhumov, Gennady Shvets, Rainer Hillenbrand. SCIENCE VOL 313 15 SEPTEMBER 2006

LIMITATIONS

- Needs a near field probe to measure

Far-Field Optical Superlens

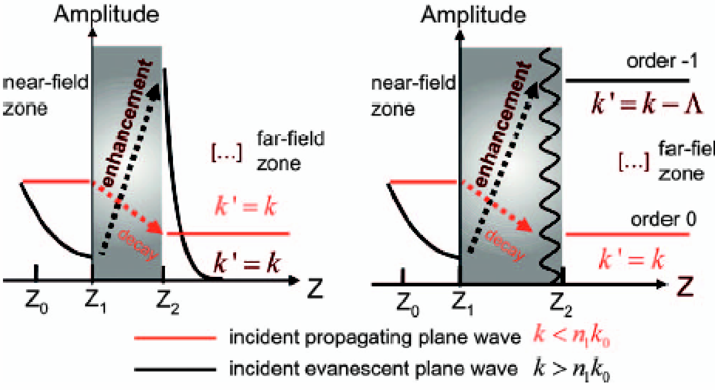

Transmitted properties of (a) a conventional superlens versus (b) a FSL. It is assumed that waves are radiated by an object at $z = z0$. Incident evanescent waves are enhanced in transmission through a conventional superlens (a) and still vanish quickly in the near-field zone, limiting the imaging ability of a superlens to the near field. In contrast, a FSL (b) both enhances and converts the original evanescent waves in propagating waves. In this latter case, incident propagating waves are comparatively transmitted with low amplitude in the far field, and the main contribution to the far-field angular spectrum is due to the incident evanescent waves. Using this property, the near- field angular spectrum can be retrieved from the measurement of the far-field angular spectrum.

Durant *et al.* Vol. 23, No. 11/November 2006/J. Opt. Soc. Am. B 2383

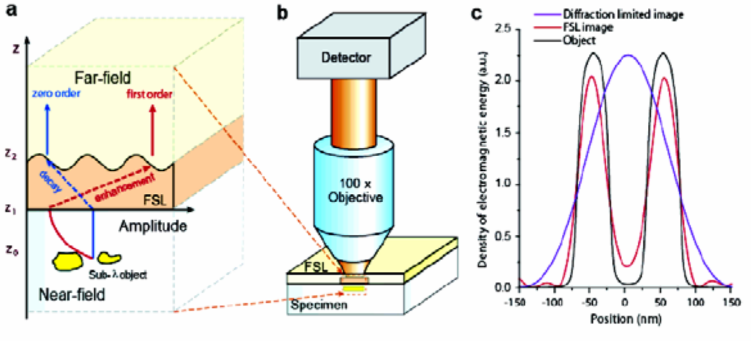

(a) A FSL. (b) Far-field superlens optical microscope can be realized by insertion of a FSL between the specimen and objective of a regular optical microscope. (c) Subwavelength object with two line sources of 50 nm width separated by a 50 nm gap and its far-field image by FSL calculated for p-polarized normally incident laser light at a wavelength of 377 nm. Calculation shows a unique subdiffraction-limited image can be obtained by FSL. A diffraction limited image from a conventional optical microscope (NA) 1.5) is also shown as comparison.

Zhaowei Liu et al NANO LETTERS 2007 Vol. 7, No. 2 403-408

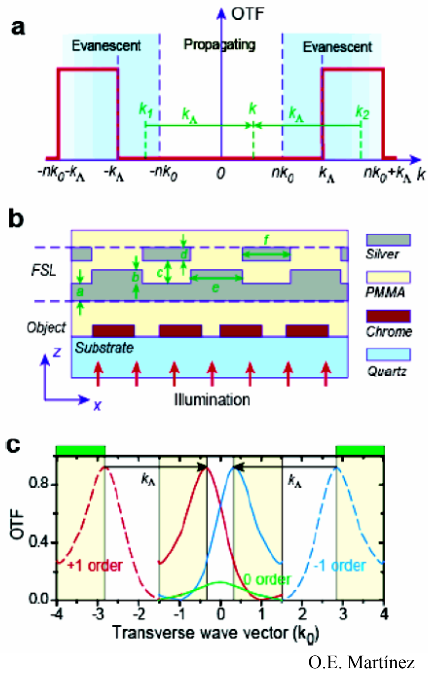

(a) Ideal OTF for FSL that enhances incident evanescent waves within wavevector bands ($nk_0 < |k| < nk_0 + k_\Lambda$ where n is the refractive index of the surrounding media and k_0 and k_Λ are the light wavevector in vacuum and grating wavevector, respectively. This ideal OTF ensures a one-to-one relationship between the measured far-field signal (k) and its evanescent origin (k_2), therefore unique imaging retrieval. (b) Schematic of a silver FSL and a chromium object fabricated on a quartz substrate. The computationally optimized geometry of the FSL is a) 35 nm, b) d) 55 nm, c) 100 nm, e) 45 nm, and f) 105 nm. (c) Calculated OTF of the optimized FSL under p-polarized incident light with vacuum wavelength of 377 nm and grating wavevector k_Λ) 2.5k0. The dashed red and blue curves represent the enhanced evanescent waves. Solid curves represent the propagating waves shifted from the evanescent waves. No wavevector mixing occurs in the shaded range ($2.8k_0 < |k| < 4k_0$) that ensures unique imaging resolution up to $4k_0$.

Zhaowei Liu et al NANO LETTERS 2007 Vol. 7, No. 2 403-408

Zhaowei Liu et al NANO LETTERS 2007 Vol. 7, No. 2 403-408

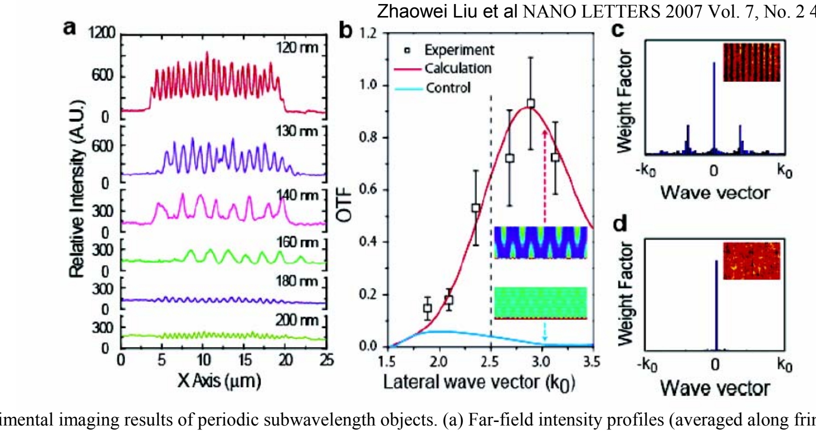

Experimental imaging results of periodic subwavelength objects. (a) Far-field intensity profiles (averaged along fringes) of six nanowire array objects under p-polarized normal illumination at 377 nm. (b) Measured OTF of the silver FSL shows a selectively enhanced band that agrees well with the theoretical calculations (red solid curve). The calculation of a simple grating by replacing the silver slab with PMMA (blue solid curve) shows a very low OTF due to the absence of evanescent wave enhancement. The upper and lower insets compare the computed field distribution after a subwavelength object with FSL and with the simple grating without silver slab, respectively (the object with 120 nm period, i.e., $k \sim 3.14k0$). A clear image can be seen from the FSL sample at the far field due to the strong evanescent enhancement via silver slab, while no such image is obtained with a simple grating. (c,d) Measured far-field patterns (inset) and their Fourier spectra for the 130 nm object under p and s polarization, respectively. As a control experiment, s polarization does not undergo the surface plasmon mediated enhancement at the FSL, resulting in no characteristics of the object at far field.

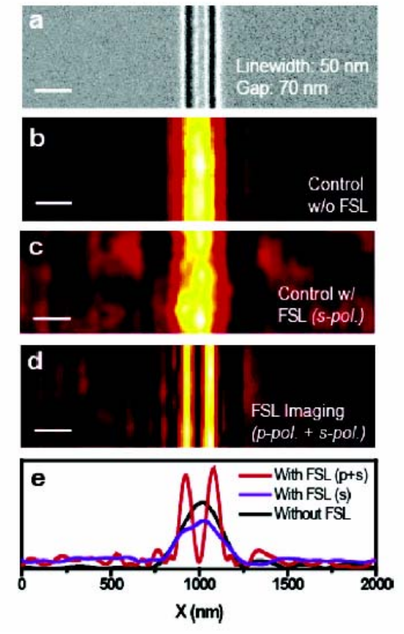

Far-field imaging of a pair of nanowires. (a) Scanning electron microscopy image of an object nanowire pair with 50 nm wide slit and 70 nm gap inscribed by focused ion beam on a 40 nm thick Cr film on the quartz substrate. (b) Diffraction-limited image from a conventional optical microscope cannot resolve the two nanowires (NA) 1.4, λ0 = 377 nm). (c) Reconstructed FSL images using s polarization is diffraction limited due to the lack of surface plasmon assisted evanescent enhancement. (d) FSL image combining both s and p polarizations that resolves the subdiffraction objects due to strong evanescent enhancement via surface plasmon excitation at FSL. The scale bars in (a), (b), (c), and (d) are 200 nm. (e) The averaged cross-section image profiles from (b), (c), and (d), respectively.

Zhaowei Liu et al NANO LETTERS 2007 Vol. 7, No. 2 403-408

Hyperlens

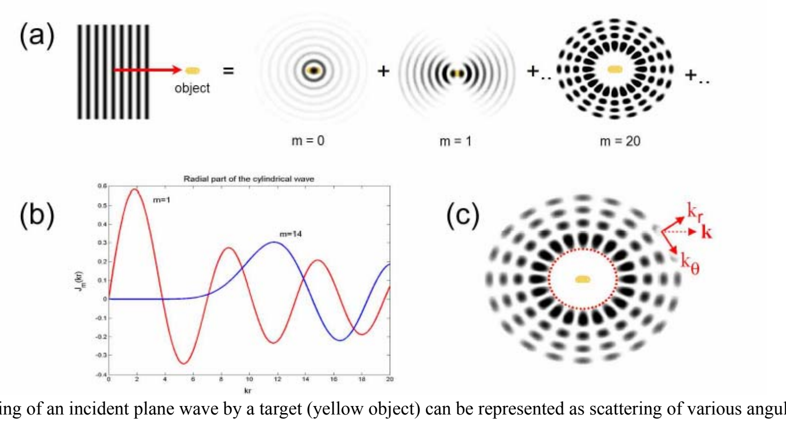

(a) Scattering of an incident plane wave by a target (yellow object) can be represented as scattering of various angular momentum modes (the regions of high intensity are shown in black and low intensity in white). Higher order modes are exponentially small at the center (b). This results from an upper bound on values of k_θ and the formation of the caustic shown in red in (c).

Zubin Jacob et al 4 September 2006 / Vol. 14, No. 18 / OPTICS EXPRESS 8247

For example a plane wave

$$\exp(ikx) = \sum_{m=-\infty}^{m=\infty} i^m J_m(kr)\exp(im\phi),$$

$$m = k_\theta r,$$

A bound appears for the radial component of k, that depends on m

$$k_r^2 + k_\theta^2 = \varepsilon \frac{\omega^2}{c^2}.$$

If anisotropic dispersion with one negative component

$$\frac{k_r^2}{\varepsilon_\theta} - \frac{k_\theta^2}{|\varepsilon_r|} = \frac{\omega^2}{c^2}$$

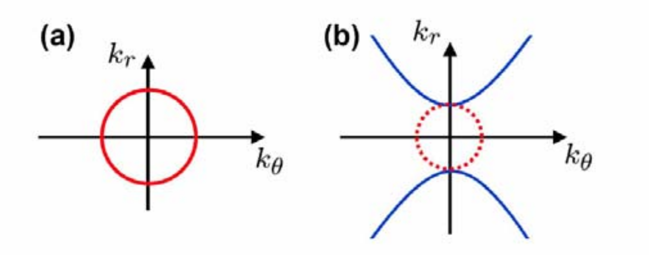

Dispersion relation for isotropic medium (a) and for a material with $\varepsilon_r < 0$, $\varepsilon_\theta > 0$ (b). Note that for a fixed frequency, the wave vector *k* can take on arbitrarily large values (within the effective medium approximation).

Zubin Jacob et al 4 September 2006 / Vol. 14, No. 18 / OPTICS EXPRESS 8247

Proposed hyperlens construction

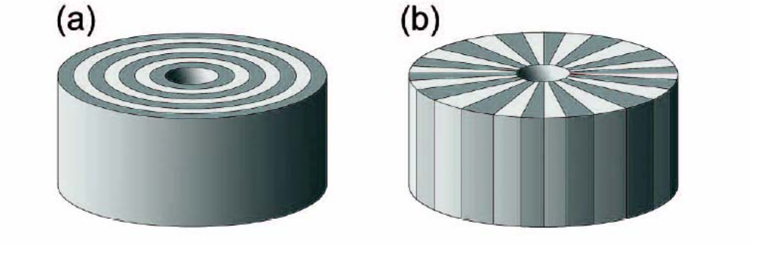

Possible realizations of metacylinders. Concentric metallic layers alternate with dielectric layers (a) or radially symmetric “slices” alternate in composition between metallic and dielectric (b) to produce ($\varepsilon r < 0$, $\varepsilon\theta > 0$) anisotropy. This results in a hyperbolic dispersion relation necessary for penetration of the field close to the center.

Zubin Jacob et al 4 September 2006 / Vol. 14, No. 18 / OPTICS EXPRESS 8247

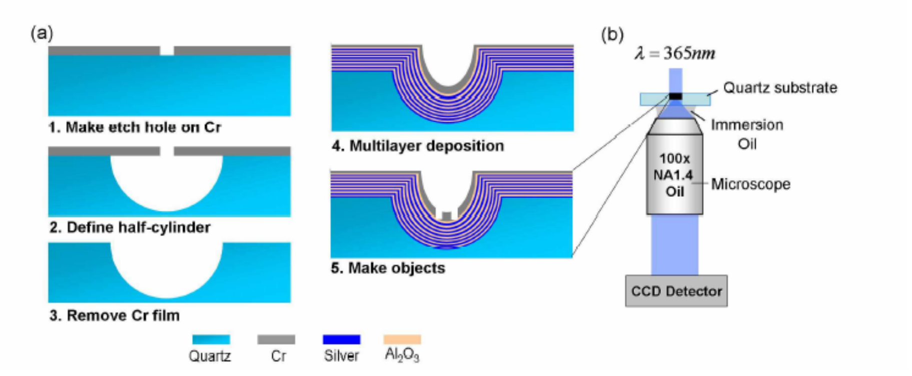

(a) Hyperlens sample fabrication process flow. Through the etch hole on a Cr film (1), isotropic wet etching makes cylindrical groove in quartz (2). After Cr film is removed (3), multilayer hyperlens structure is fabricated using alternate deposition of Ag and Al_2O_3 (4). A Cr film caps the hyperlens structure for object fabrication (5). (b) Imaging setup. Completed hyperlens/object sample is placed under objective with incident light at 365nm, conventional far field microscope with 100X oil immersion objective and UV sensitive CCD detector was used for direct far field imaging.

Hyesog Lee et al 26 November 2007 / Vol. 15, No. 24 / OPTICS EXPRESS 15886

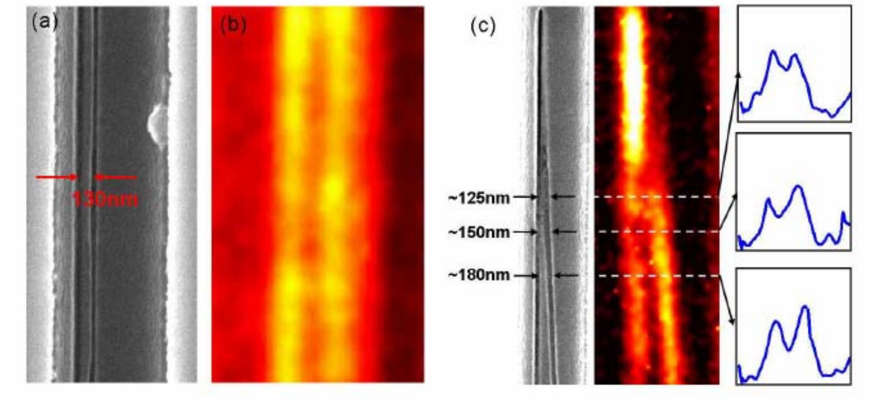

. Hyeperlens imaging results. (a) SEM image of 130nm line pair object on Cr film. Dark region is the hyperlens and the bright region is the flat surface. (b) Image captured by optical microscope through hyperlensing shows 130nm gap is clearly resolved. (c) Left: SEM image of tilted line pair object with indicated gap sizes. Middle: Image captured by optical microscope through hyperlensing. Right: Intensity profiles of the three indicated cross sections showing resolved 125nm gap (top).

Hyesog Lee et al 26 November 2007 / Vol. 15, No. 24 / OPTICS EXPRESS 15886

Radiationless Electromagnetic Interference: Evanescent-Field Lenses and Perfect Focusing

R. Merlin/ 12 July 2007 / Page 1 / 10.1126/science.

$f_{q_0} e^{i\kappa(q_0)z}$ $\quad M(\rho)\times f_{q_0}(\rho)$

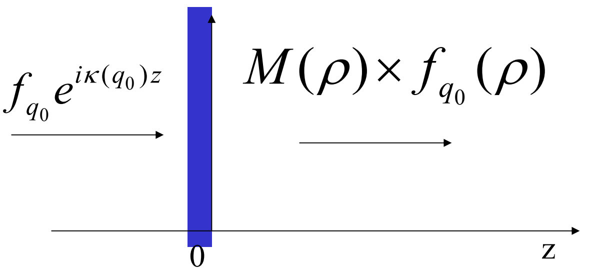

If M has a pole at iL will produce a near field focus at

z=L

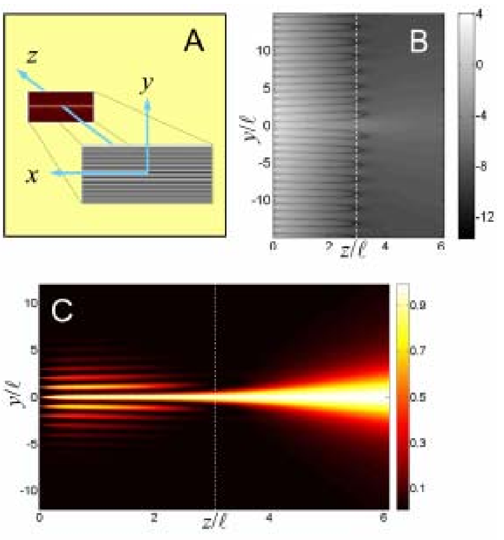

Fig. 2. Radiationless nterference. (**A**) Schematic showing a subwavelength plate, represented as a modulated array of linear current sources at z = 0 and the plane showing the focalline. L/l =3. (**B**) Contour plot of $\ln|H_y|$. (**C**) Contour plot of $|Hy(z,y)/Hy(z,0)|^2$ The dashed white line at $z = L$ denotes the focal plane.

Conclusions

- Nanoimaging with light is a mature field
- Applications to life sciences is just beginning
- Many more techniques should be expected

THE NANOPEOPLE IN THE LAB

NFO 10
BUENOS AIRES - ARGENTINA

www.nfo10.org

September, 1st - 5th, 2008 // Buenos Aires, Argentina
Salguero Plaza - Jerônimo Salguero 2686 - Ciudad de Buenos Aires

10th International Conference on Near-field Optics, Nanophotonics and related techniques

TOPICS

Plasmonics
Nanophotonics (building blocks, devices, circuits)
Near Filed Enhancement and applications (Raman, nonlinear)
Nonlinear and ultrafast
Nanofabrication
Antennas
Metamaterials and superlensing
Applications to Biology and Chemistry
Instrumentation and probes
Spectroscopy
Quantum systems, semiconductor physics and materials science
Single particles (molecules, nanoparticles)
IR and THz
Cavity nano-optics, plasmonic and photonic crystals
Nanoscale photothermal phenomena
Novel concepts and phenomena

BONUS

September 1st , one day school
"Introduction to Nano-Optics"

IMPORTANT DATES

Abstract Submission: April, 30th
Early Registration: June, 15th

CONTACT

Chairs:
Oscar E. Martinez
(Universidad de Buenos Aires)
Andrea V. Bragas
(Universidad de Buenos Aires)
Email
nfoptics10@gmail.com

155